Chem Soc Rev

This article was published as part of the

From microfluidic application to nanofluidic phenomena issue

Reviewing the latest advances in microfluidic and nanofluidic research

Guest Editors Professors Albert van den Berg, Harold Craighead and Peidong Yang

Please take a look at the issue 3 table of contents to access other reviews in this themed issue

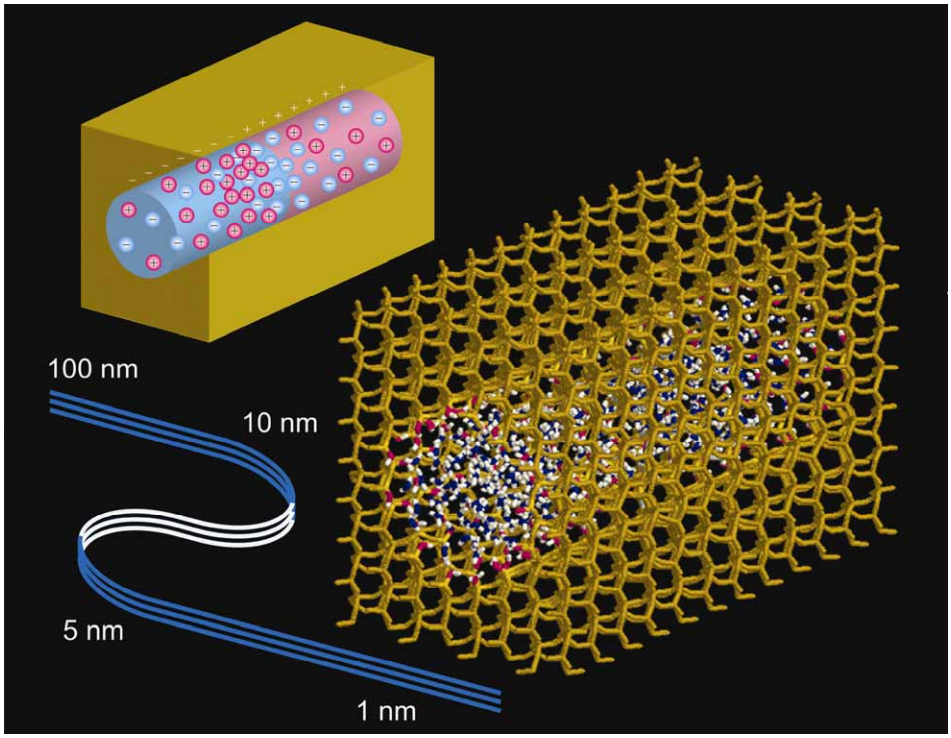

Theory and experiments of concentration polarization and ion focusing at microchannel and nanochannel interfaces†

Thomas A. Zangle, Ali Mani and Juan G. Santiago*

Received 5th August 2009
First published as an Advance Article on the web 29th January 2010
DOI: 10.1039/b902074h

In this *tutorial review* aimed at researchers using nanofluidic devices, we summarize the current state of theoretical and experimental approaches to describing concentration polarization (CP) in hybrid microfluidic–nanofluidic systems. We also analyze experimental results for these systems and place them in the context of recent theoretical developments. We then extend the theory to explain the behavior of both positively and negatively charged, low-concentration, analyte species in systems with CP. We conclude by discussing several applications of CP in microfluidics.

1. Introduction

A variety of fabrication techniques are now available to construct nanofluidic devices and interface them with microfluidic systems.[1–4] This has motivated the study of nanofluidic devices as modules within microfluidic systems to, for example, preconcentrate analytes[1,5,6] or detect and analyze DNA.[7] However, application of an electric field across a nanofluidic device creates regions of enriched and depleted (net neutral) ion concentration, an effect called concentration polarization (CP). CP can change the conductivity and electric field in adjoining microchannels by orders of magnitude[8] which, in turn, influences sample transport throughout these systems.[9,10] Recent work has shown that CP enrichment and depletion zones can propagate through hybrid microchannel–nanochannel devices and profoundly affect the global behavior of the system.[2,11]

A large number of experimental studies[1–3,5,8,10,12–27] have addressed the influence of CP on the transport of an analyte ion with a concentration relatively low compared to the concentration of background ions in hybrid microfluidic–nanofluidic systems. To date we know of only two papers which have attempted to explain and categorize several of these experimental results. However, the first is only a preliminary work we published on this topic,[10]and the second consisted of a (transient) one-dimensional computational model.[9] In this paper we extend recent theoretical developments[11] to provide a more generalized analytical framework for understanding the effects of CP on both background and analyte ion transport in hybrid microfluidic–nanofluidic systems.

We first review nanochannel physics as it relates to CP (section 2). Second, we briefly discuss historical CP work and introduce the recent literature (section 3). Third, we summarize the analytical CP theory recently presented by Mani *et al.*[11] (section 4). Sections 5 and 6 then describe the effects of CP on cationic and anionic analytes, respectively, in systems with

Stanford University Mechanical Engineering Department, Building 530, Room 225, 440 Escondido Mall, Stanford, California 94305-3030, USA. E-mail: juan.santiago@stanford.edu
† Part of the themed issue: From microfluidic application to nanofluidic phenomena.

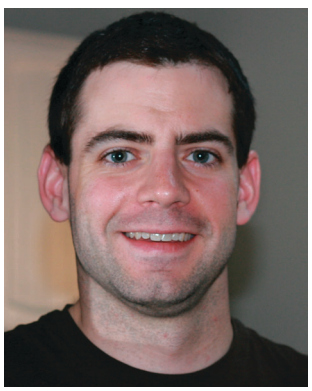

Thomas A. Zangle

Thomas A. Zangle is a PhD candidate in the Mechanical Engineering Department at Stanford University, under the guidance of Prof. Juan G. Santiago. He was the recipient of the Regina Casper Stanford Graduate Fellowship. He received his MS in Mechanical Engineering from Stanford and his A.B. and BE degrees in Engineering Sciences from Dartmouth College. His research at the Stanford University Microfluidics Laboratory focuses on experimental, theoretical and fabrication aspects of the integration of nanofluidic devices into microfluidic systems.

Ali Mani

Ali Mani is a research associate at Stanford's Center for Turbulence Research and the Flow Physics and Computational Engineering group in the Mechanical Engineering Department. He earned his PhD in mechanical engineering from Stanford University in 2009. His research interest is in multiphysics problems in fluid mechanics relating to electrokinetics, turbulence, waves, and interfaces. He primarily uses mathematical models and numerical techniques to study detailed physical processes in these systems. His publications span across different disciplines in fluid mechanics including aero-optics, micro/nano-fluidics and aeroacoustics.

negatively charged nanochannel walls (we will focus all of our discussions on the case of negatively charged walls). Finally, section 7 briefly discusses several applications of CP effects in microfluidics.

Note that in this review, we consider electrokinetic CP in microchannel systems caused by forcing a current through a nanochannel or a nanoporous membrane. There are at least two other physical phenomena which are commonly referred to as concentration polarization and which are not the topic of this review. These include solute buildup at a (steric) filter membrane[28] or performance losses in a fuel cell due to the concentration of reactants.[29]

In our discussion of low concentration analyte ions, we will examine electrokinetic preconcentration at microchannel–nanochannel interfaces. However, we note that other preconcentration modes are possible. For example, Foote *et al.*[30] fabricated silica nanoporous membranes and preconcentrated proteins using size exclusion. Similarly, Meagher *et al.*[31] used a size-exclusion preconcentrator to improve the limit-of-detection of an on-chip immunoassay from 300 pM to <10 pM. For a more thorough overview of size exclusion techniques using nanoporous membranes and nanochannels, see the recent review by Han *et al.*[32] We note, however, that CP has been observed to influence the performance of nanoporous membranes (including size-exclusion-based systems) under conditions in which the nanoporous membrane is charged. Hlushkou *et al.*[22] reported on the preconcentration efficiencies at charged and uncharged nanoporous membranes and found that much higher field strengths are required to achieve the same preconcentration factor with charged membranes due to the CP depletion region. This depletion zone acts as a large electrical resistance, increasing the required applied electric potential. In a paper on an integrated size-exclusion preconcentrator, Hatch *et al.*[6] reported a decrease in current with time due to growth of an anode-side, CP depletion zone; this had an adverse effect on repeatability of the subsequent separation in polyacrylamide sieving matrix. A similar effect has been observed in DNA capillary separation though a gel.[33] CP effects in membrane preconcentration can perhaps be mitigated by avoiding trans-membrane current during a separation step (following a size-exclusion preconcentration)[6] or by applying current through the membrane only for a short time.[31]

Juan G. Santiago

Juan G. Santiago is Associate Professor of Mechanical Engineering at Stanford University and Chair of the Thermosciences Group. He specializes in microscale transport phenomena and electrokinetics. He earned his PhD in Mechanical Engineering from the University of Illinois at Urbana-Champaign. Among other awards, he won the National Science Foundation Presidential Early Career Award for Scientists and Engineers (PECASE) ('03–'08). Santiago has presented 13 keynote and named lectures and over 100 additional invited lectures. His group has been awarded nine best paper and poster awards. He has authored/co-authored over 100 archival publications, authored/co-authored 200 conference papers, and holds 25 patents.

2. Nanochannel physics and CP

The physics of electrokinetics in nanochannels are discussed elsewhere[4,34–36] and will not be reviewed at length here. Instead, we present here brief scaling arguments which highlight key physical effects. CP occurs when current flows into or out of an electric double layer (EDL) shielding a charged surface. The common case is when ionic current passes from a microchannel into a nanochannel. In the nanochannel, a significant portion of the current is carried by the EDL which, unlike the bulk solution, has an appreciably different number of negative *versus* positive charges. This deviation from bulk conductance is well known and has been characterized experimentally.[34–36] We can use a formulation of this deviation from bulk conductance to show that the primary parameter that governs CP is a type of Dukhin number, relating bulk and surface conductances. This is consistent with the analytical model we presented in ref. 11 in which a type of Dukhin number appears as a nondimensional parameter in the differential equations governing CP. This is also consistent with our experimental results showing that a Dukhin number can be used to accurately predict the behavior of CP enrichment and depletion regions.[2]

Neglecting for the moment current due to diffusive fluxes, ion current through a wide, shallow (micro or nano) channel can be written as a sum of advection and electromigration current as:

$$I = w\sum_i \left[\int_0^h (Fz_i c_i(y)U^{\text{bulk}}(y))\mathrm{d}y + \int_0^h (F^2 z_i^2 \nu_i c_i(y)E)\mathrm{d}y,\right] \tag{1}$$

where w is the width of the channel; h is the channel height; F is Faraday's constant; z_i, and ν_i, are the valence and mobility of the i^{th} species; c_i is the concentration of the i^{th} species which can vary with channel location; E is the external electric field; and U^{bulk} is the bulk velocity. In the thin electric double layer (EDL) limit the total channel conductance, $G_{\text{tot}} = I/E$ can be estimated for a symmetric electrolyte as:

$$G_{\text{thinEDL}} \approx 2F^2 z^2 \nu c_0 w h, \tag{2}$$

where c_0 is the concentration outside of the EDL. Eqn (2) is the definition of bulk conductance, so $G_{\text{thinEDL}} = G_{\text{bulk}}$. Similar to the analysis of Stein *et al.*,[34] and for simplicity, we impose a boundary condition of constant and uniform wall charge, σ, and take the limit of eqn (1) for thick EDLs (*i.e.*, the limit of $h/\lambda_{\text{D}} \ll 1$), we obtain an expression for the surface conductance:

$$G_\sigma \approx |\sigma| 2Fz\nu w\left(1 + \frac{|\sigma|h}{6Fz\nu\eta}\right). \tag{3}$$

In eqn (3), the second term in parentheses indicates the effects of electroosmotic transport on current and is briefly derived in Appendix I. Schoch *et al.*[36] modeled the total conductance of a nanochannel as the sum of a bulk conductance term (as in eqn (2)) and a surface conductance term (as in eqn (3) but without the advective current component) and found a good fit to experimental data. Following this approach, and neglecting the advective current contribution, we can take the ratio of eqn (2) to the leading term of eqn (3) to obtain a good indication of the relative importance of bulk conductance, G_{bulk}, to surface conductance, G_σ:

$$\frac{G_{\mathrm{bulk}}}{G_\sigma} \approx \frac{Fhzc_0}{\sigma}. \qquad (4)$$

Eqn (4) is an inverse Dukhin number for a symmetric electrolyte, and is equal to the more general parameter used by Mani *et al.*[11] and Zangle *et al.*[2] in descriptions of CP. This scaling has also been noted by Kim *et al.*[1] for microchannel–nanochannel CP and Lyklema[37] for CP around a spherical particle.

Importantly, CP depends primarily on the Dukhin number, and not the ratio of channel height to the Debye length, h/λ_d.[2,11] We note h/λ_{d} is often quoted as a key parameter in the determination and characterization of CP, but we find this parameter is in fact not nearly as useful as $Fhzc_0/\sigma$, which relates the number of ions in the bulk to the number of ions

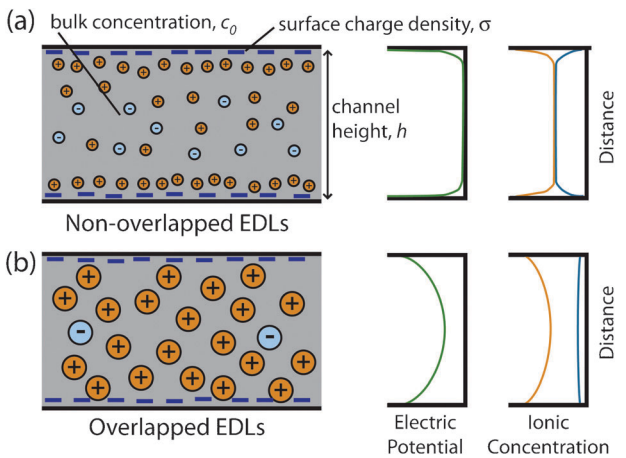

Fig. 1 Schematic of channels with (a) non-overlapped electrical double layers (EDLs) and (b) overlapped EDLs. In channels with EDLs of finite thickness (b), there can be a much greater concentration of positive ions than negative ions. If the EDLs are overlapped, then the potential at the center of a channel does not fall to zero. In a channel with non-overlapped EDLs (a), the electric potential caused by the wall charge falls to zero at the center of the channel. However, the total number of counter-ions to the wall charge(positive ions for negatively charged walls) can still be much greater than the concentration of co-ions when $Fhzc_0/\sigma$, (where c_0 is bulk concentration, h is channel height h, F is Faraday's constant and σ is surface charge density) is significantly smaller than unity. $Fhzc_0/\sigma$ is similar to an inverse Dukhin number, describing the number of ions in the center of the channel relative to the number of ions associated with the EDLs. We note that strong CP effects have been demonstrated in literature for systems with non-overlapped EDLs and $Fhzc_0/\sigma \ll 1$.[26] Figure adapted with permission from Karnik *et al.*[62] Copyright 2005 American Chemical Society.

associated with EDLs. Furthermore, we note that overlapped EDLs (h/λ_d of order unity or less) are often cited as a requirement of (or as being correlated with) CP,[5,8,14,19,21] but this is simply not true. From simple Boltzmann distribution arguments, EDL mobile counter ion density scales as $c_0 \exp(-\zeta ez/kT)$ where ζ is the zeta potential and c_0 is the bulk concentration far from the wall.[11,38] For typical glass or silica surfaces, with zeta potentials of roughly −100 mV, this implies near-wall counter ion densities can be order 50-fold higher than the bulk. Therefore, as shown in Fig. 1, such systems can have values of $Fhzc_0/\sigma$ significantly smaller than unity even for h/λ_d values of 10 or more. For example, strong CP effects have been reported for h/λ_d values of greater than 100.[26]

3. Concentration polarization models and experiments

CP has been studied extensively in the context of colloids[37,39] and membranes.[40–42] In early work on membrane CP, Block and Kitchener[40] studied nanoporous materials and speculated on the role of water dissociation in the low-concentration depletion regions. In a seminal CP contribution, Dukhin and Shilov[39] presented a simplified description of CP based on a model with very thin EDLs that carry current due to surface conduction. Their model showed that CP occurs when electric field lines cross from net neutral, bulk solution, into electrical double layers. More recent work has shown that electrokinetic instabilities can cause systems with nanoporous membranes to have higher (“overlimiting”) conductance than the limit dictated by ion diffusion.[43] Tallarek and coworkers have examined CP in beds of porous beads and glass monoliths.[13,27] See the review by Höltzel and Tallarek[44] for more information on CP around nanoporous membranes, packed beds, and glass monoliths.

In microfluidic systems, Pu *et al.*[14] showed the first reported visualization of CP near nanochannels and presented a qualitative model describing CP. Major themes of research on microfluidic–nanofluidic interfaces since this work have been the study of recirculation zones and the effects of CP on the concentration of ionic species. We will briefly introduce this research in sections 3.1 and 3.2, before going into much greater detail on CP effects on ion concentration in sections 4, 5 and 6.

3.1 Recirculation effects

Recirculation near microfluidic–nanofluidic interfaces has been noted in several studies[8,11,19,45,46] and at least three different physical origins of this recirculation have been noted. Park *et al.*[45] presented an analytical model suggesting two different mechanisms for the formation of vortices at a gradual microchannel to nanochannel constriction. Though this model neglects the effects of CP on the background electrolyte concentration, it does capture two possible mechanisms for vortex generation at a microchannel–nanochannel interface. First, surface conductance causes the ratio of ionic current to bulk flow to vary with changes in the channel cross-sectional area. Second, the effects of finite EDLs cause the electroosmotic flow (EOF) velocity profile to be non-uniform across a microchannel–nanochannel interface. Both of these effects create internal pressure gradients. The analysis of Park *et al.*

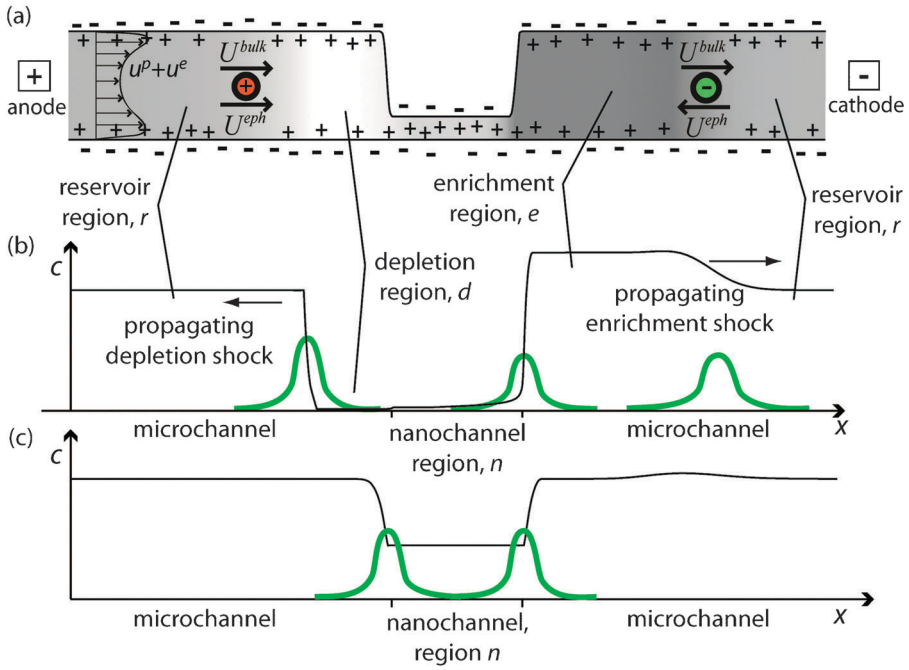

Fig. 2 Schematic showing various possibilities of anionic species focusing or stacking in a typical microchannel–nanochannel geometry. (a) shows a typical microchannel–nanochannel–microchannel layout with enrichment and depletion of the background electrolyte (BGE) shown as a greyscale map (darker regions correspond to enrichment). The 'reservoir' region is the section of microchannel which is not yet affected by progress of the CP front; therefore, the concentration of each ion in this region is equal to the concentration inside of the end-channel reservoir (not shown). Focusing of a low-concentration anionic species occurs in zones where the sum of the electrophoretic and (area-averaged) bulk velocities are locally zero with a negative divergence.[47] For counter-ionic (positive for negatively charged walls) species, focusing is not possible since these species always have positive total velocity. The black curve in (b) shows computed BGE concentration from a propagating CP case.[2] The green peaks represent possible focusing or stacking zones for a low concentration anionic analyte,‡ whose concentration is much lower than the BGE. The black curve in (c) shows a computed no-propagation case.[2] Here we show two possible focusing locations for analyte anions.

demonstrates that these internal pressure gradients can create vortices at the channel centerline, along the channel walls, or in both regions.[45] Similar vortices were noted in the computational results of Mani *et al.*[11] and Postler *et al.*[46] The latter two studies found that an adverse pressure gradient can lead to local flow reversal and the formation of eddies near microchannel–nanochannel interfaces. Postler *et al.*[46] also examined the coupling of CP and electroosmotic flow.

The work of Zaltzman, Rubinstein, and co-workers[41,43] suggests that electrokinetic flow instability is another possible mechanism for the formation of vortices at a microfluidic–nanofluidic interface. This work has focused on nanoporous membrane systems in which current is observed to initially increase linearly with increasing applied electric field up to a point where current through the membrane becomes limited by diffusion through the depletion region. This is called the "limiting current" regime. Zaltzman, Rubinstein, *et al.*[41,43] demonstrated that a fluid instability is responsible for mixing the depletion region (with fluid regions of less depleted ion density) at electric fields beyond the limiting current regime. Mixing due to instability at high electric fields reduces the resistance of the depletion region, resulting in a notably higher current through the nanoporous membrane, which is called "overlimiting current." See Zaltzman *et al.*[43] for more details on overlimiting current in membrane systems. Kim *et al.*[19] studied overlimiting currents in microchannel–nanochannel systems and found that the observed behavior of analyte molecules in the depletion region was correlated to changes from limiting to overlimiting current behavior. Recent work by the same group[8] studied the physics of the depletion region in a nanofluidic preconcentrator where recirculation was observed. From measurements made using microfabricated electrodes the authors estimated the electric field in the depletion region to be up to 33 times higher than the nominal electric field applied to their device.

3.2 Work describing ion concentration

Plecis *et al.* described different focusing and stacking‡ regimes of analyte species using a computational model which we will discuss in more detail below.[9] In simultaneous work, we presented stacking and separation of two low concentration anionic species on a CP enrichment shock.[10] These two species were assumed to be present in low concentration relative to the background electrolyte (BGE) so that they do not affect the dynamics of CP and the axial electric field. Zangle *et al.*[10] included an analytical model for stacking of an anionic species

‡ Consistent with Bharadwaj *et al.*,[47] we use focusing to describe the condition where there is a focal point for the analyte. A focal point is a point or region in some reference frame where the drift velocity of the focused species changes sign so that sample is driven to the focal point. We use "stacking" to describe the less stringent situation where an analyte drift velocity decreases in magnitude (causing an increase in concentration) as the analyte migrates through some stacking region containing an electric field gradient.

on the enrichment shock. In the following sections, we will present a generalization of this model which describes ion behavior at each region indicated in Fig. 2. Fig. 2 shows computations[2] for the concentration of a background electrolyte (dominant ion) in a microchannel–nanochannel system resulting from CP as black lines. Green peaks indicate schematically possible focusing or stacking locations of an anionic analyte.

We also recently presented an analytical description of the behavior of the background electrolyte (BGE) in microchannel–nanochannel systems.[2,11] In particular, our model shows that, under certain conditions, enrichment and depletion zones in a microfluidic system propagate outwards from nanochannel interfaces. We supported our model with experiments and computations and found it to be a good qualitative predictor of the behavior of CP zones, and a fair-to-good predictor of the quantitative limits of the associated regimes. In order to provide a framework for comparing as many experimental cases as possible, we will use the most general analytical theory of CP in a channel system to date, which was presented by Mani *et al.*[11] We will first look at experimental results in the context of this binary electrolyte theory's predictions of CP propagation. Then we will extend the theoretical results to predict the behavior of specific low concentration counter-ionic and co-ionic analyte species in a microchannel–nanochannel system.

4. Propagating *vs.* non-propagating CP and nanochannel ion concentration

In this section, we summarize the physical regimes which lead to the propagation of CP zones away from nanochannels and regimes which lead to non-propagating CP. In a two-paper series, Mani *et al.*[11] and Zangle *et al.*[2] developed and tested a simplified model of charged species transport in a series microchannel–nanochannel–microchannel system. We showed that concentration polarization (CP) enrichment and depletion zones will propagate as shock waves if the following condition is satisfied:

$$c^*_{0,r}h^*_n < \max(\nu^*_2, 2\nu^*_2 - 1) \tag{5}$$

where $c^*_{0,r}h^*_n = (\nu_1 z_1 - \nu_2 z_2)Fh_n c_{0,r}/(-2\nu_1\sigma)$ is an inverse Dukhin number which describes the ratio of bulk to surface conductance, and $\nu^*_2 = \nu_2 z_2 F\eta/\zeta_n\varepsilon$ is the mobility of the co-ion (to the wall charge) nondimensionalized by the electroosmotic mobility. Here, $c_{0,r}$ is the BGE reservoir concentration. h_n is the nanochannel height; ν_1 and ν_2 are the mobilities of the positive and negative species; z_1 and z_2 are the valences of the positive and negative species, σ is wall charge, ξ is the zeta potential, F is Faraday's constant, ε is permittivity and η is viscosity.

The enrichment and depletion shock waves predicted by Mani *et al.*[11] are sharp, propagating boundaries between regions of the microchannel where concentration has been influenced by the nanochannel and regions which are still at the initial, reservoir concentration. These shocks are clearly seen in plots of concentration *versus* time and axial dimension as in Fig. 3 below. In Fig. 3, the depletion shock on the left separates the low concentration (black) depletion region from undisturbed regions. Similarly, the enrichment shock on the right is the moving boundary between the high concentration (white or yellow) region and the undisturbed region. For a constant applied current through the nanochannel, these shocks will propagate at constant rates to the reservoirs at the end of the microchannels.[2]

Mani *et al.*[11] gave predictions of both the dynamics and steady state values of ion concentrations in the microchannel and the nanochannels. For non-propagating CP, the final values achieved in the microchannel and nanochannel are

$$c^*_{0,d} = c^*_{0,e} = c^*_{0,r} \tag{6}$$

where the subscripts d, e, r and n refer to the regions shown in Fig. 2. For propagating CP, there are two relations corresponding to two ranges of $\nu^*_{2,n}$. For propagating CP with $\nu^*_2 < 1$,

$$c^*_{0,d} = c^*_{0,n} = 0 \text{ and } c^*_{0,e} = \nu^*_2/h^*_n \tag{7}$$

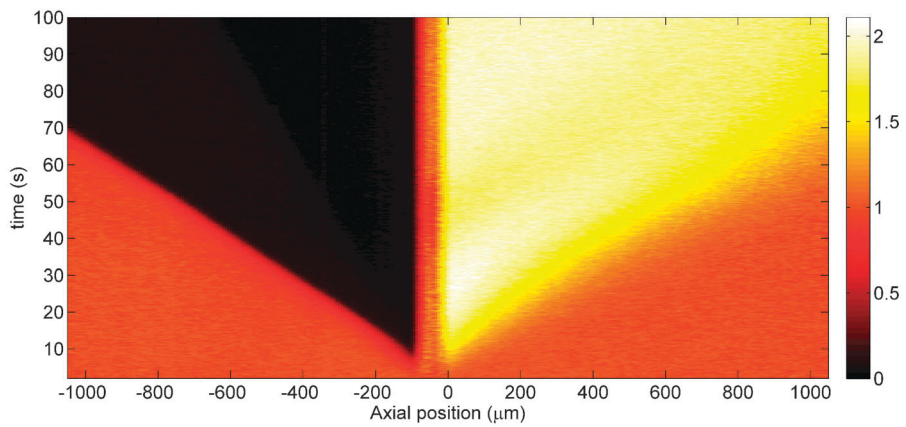

Fig. 3 Experimental spatiotemporal data showing enrichment and depletion shock waves emanating from both sides of a nanochannel between two microchannels. This plot shows width-averaged fluorescence intensity (using a colormap) as a function of axial position (x-axis) and time (y-axis). An electric field was applied from left (anode) to right (cathode). In this constant-current experiment the enrichment region spreads towards the cathode (on the right) at constant velocity and the depletion region spreads at constant velocity towards the anode (to the left). The nanochannel is located between $x = -100$ and 0 μm. Adapted with permission from Zangle *et al.*[2] Copyright 2009 American Chemical Society.

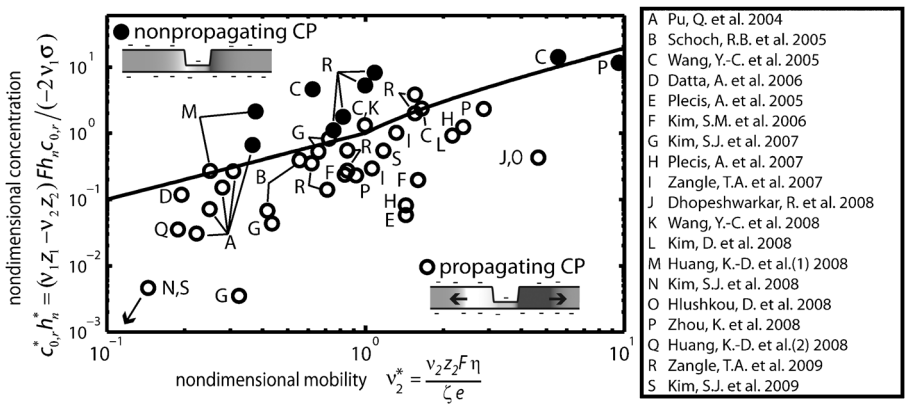

Fig. 4 Propagating *versus* non-propagating CP: Analytical predictions and experimental results. Propagating CP is predicted when the experimental condition lies below the solid line phase boundary, as predicted by Mani *et al.*[11] Symbols are data from 56 sets of reported experiments representing 43 unique values of ν_2^* and $c_{0,r}^* h_n^*$ pairs.[1–3,5,8,10,14–26] Open symbols represent reported results consistent with propagating CP, closed symbols represent results consistent with non-propagating CP. Two reported propagating cases, N and S, lie out of the range of this figure (each used highly charged Nafion 117). The analytical model is a fairly good predictor of the propagation regime.

While for propagating CP with $\nu_2^* \geq 1$, we have

$$c_{0,d}^* = \frac{(\nu_2^* - 1)^2}{[(2\nu_2^* - 1)h_1^*]},$$
$$c_{0,n}^* = (\nu_2^* - 1)/h_n^* \text{ and} \qquad (8)$$
$$c_{0,e}^* = (2\nu_2^* - 1)/h_n^*.$$

The final concentrations inside microchannels and nanochannels given by eqn (6)–(8) in turn establish the electric field distribution in a microchannel–nanochannel systems with CP. In the following sections, we will use these results to predict the behavior of species which are in low-concentration relative to the background electrolyte (BGE) and which are either counter- or co-ions to the wall charge. In effect, these final ion concentration values will in part determine if and where a low concentration analyte species focuses or stacks.

The existence condition for propagating CP defined by eqn (5) is plotted as a solid line in Fig. 4. The region below this phase line indicates conditions which lead to CP with propagation, while the region above denotes non-propagating CP. The phase line is plotted here over the range of most interest in experiments (see discussions of experimental data below). The mobility ratio ν_2^* is typically between 0.1 and 10, since electrophoretic and electroosmotic mobilities are typically within a factor of 10 of each other. The parameter with greatest influence is $c_{0,r}^* h_n^*$, the bulk-to-EDL conductance ratio. This parameter is proportional to nanochannel height and BGE reservoir concentration and inversely proportional to surface charge density; so that interesting values span more than 4 orders of magnitude.

In Fig. 4 we also compare eqn (5) to published results from 56 sets of experiments reported in the literature. These data represent 43 unique values in the ν_2^* *vs.* $c_{0,r}^* h_n^*$ phase plot. For each experimental result, if the reported and/or presented data indicated propagating CP, then we show that data point in Fig. 4 with an open symbol. We used a closed symbol for reports indicating non-propagating CP.§ Zeta potentials for SiO_2, PET and PDMS were estimated using the data and curve fits in Kirby *et al.*[48,49] Zeta potential for HEMA hydrogel[21,22] was estimated using data from Kuo *et al.*[50] and You *et al.*[51] and a curve fit of the form $\xi/\log(c) = A \cdot pH + B$.[49] Zeta potential of Nafion 117 was estimated using data from Ge *et al.*[52] and Daiko *et al.*[53]

Fig. 4 shows that the analytical theory of Mani *et al.*[11] is a fairly good predictor of propagation behavior despite the simplifying assumptions made in deriving the model (for instance, the model assumes EDLs which are infinitely thin but which carry significant current, therefore, the definition of ν_2^* does not include any nanochannel height effects). Because the model is presented in terms of two non-dimensional parameters, it is useful as a design tool for a wide range of experimental conditions. Fig. 4 also shows that $c_{0,r}^* h_n^*$, a nondimensional concentration (inverse Dukhin number), is the major parameter determining propagating *vs.* non-propagating CP. The parameter $c_{0,r}^* h_n^*$ varies over many orders of magnitude, while ν_2^* is typically of order unity. Therefore, to avoid the effects of propagating CP, a rule of thumb is to keep $c_{0,r}^* h_n^* \gg 1$. If propagating CP is desirable for operation of a microchannel–nanochannel device, as is the case with some nanofluidic preconcentrators,[1,3,5,17] then the rule of thumb is to insure that $c_{0,r}^* h_n^* \ll 1$. In cases where $c_{0,r}^* h_n^* \sim 1$ the designer should either consult the analytical theory[11] or perform a computation using the specific conditions to be used.[2,9,11,21]

As noted earlier, this theory assumes infinite PeL/h. Mani *et al.*[11] provide a brief description of the effects of finite PeL/h on propagating CP. PeL/h effects may play a role in some reported observations including, for example, enrichment

§ Most reported experiments show visualization of a fluorescent species in low concentration relative to a non-fluorescent background electrolyte. Therefore, in such cases we looked for evidence of propagating or non-propagating CP of the background electrolyte by observing the behavior of the fluorescent analyte species. The expected behaviors for low concentration (analyte) species in propagating and non-propagating CP are described in sections 5 and 6 below.

regions which first propagate and then stop in series microchannel–nanochannel–microchannel devices.[22] Additionally, Plecis *et al.*[9] showed that the applied potential is an important component of the regime 'map' of possible preconcentration modes. This suggests that, in addition to the two nondimensional parameters considered in this description of the background electrolyte, ν_2^* and $c_{0,r}^* h_n^*$, a third nondimensional parameter related to diffusion effects may be important. Based on the results of Plecis *et al.*[9] and the description of Peclet number effects in Mani *et al.*,[11] we suggest that this additional parameter may be a Peclet number, which likely controls the thickness of enrichment and depletion shocks.

In the next sections we will extend the results from Mani *et al.*[11] to describe the behavior of ionic species which are in low concentration relative to the background electrolyte (BGE). We will assume that the concentration of these ions is low enough (relative to the BGE) that they do not affect the electric field. We will call these species cationic or anionic analytes and, for simplicity, will only consider a system with negative wall charge. However, our approach is easily extendable to a system with positive wall charge.

5. Stacking of cationic analytes

In this section, we present a model to predict the behavior of a cationic analyte (a positively charged species which is in low concentration relative to the background electrolyte). Several investigators have reported experiments with low concentrations of positively charged Rhodamine 6G[12,14,19,23,24,27] or Rhodamine 123[1] in a system with negatively charged nanochannel walls. Therefore, in this section we will analyze systems using these two fluorescent dyes as representative cationic analytes to test the analytical model predictions.

Cationic analytes electromigrate in the direction of the bulk flow and, so, in a linear microchannel–nanochannel system with negative wall charge, the cation's total species velocity in the frame of reference of an interface (the sum of the electrophoretic and bulk velocities, $U_i^{\text{eph}}/U^{\text{bulk}}$, minus the interface velocity V^{int}) is always positive; and so the cation cannot focus in a microchannel–nanochannel system with CP.¶ Cationic analytes, however, can stack (*i.e.*, increase in concentration as they traverse some interface due to a decrease in total species velocity, U_i^{tot}) or undergo electromigration dispersion (decrease concentration as they traverse some interface due to an increase in total species velocity, U_i^{tot}). We describe the behavior of cationic analytes by following an approach similar to that of Chambers *et al.*[54] who analyzed the analogous situation of ions which move through but do not focus in isotachophoretic (ITP) zones.‖ Our analysis uses the analytical results of Mani *et al.*[11] to describe the background electrolyte (BGE) concentration and electric field everywhere in a microchannel–nanochannel–microchannel system. Then, we determine the concentration of cationic species which is required to balance the total flux across each interface in the system. Note that in this system the only interfaces where the total species velocity can change are the depletion shock, microchannel–nanochannel interfaces and the enrichment shock as shown in Fig. 5. Because cationic species move from the anode to the cathode, we assume that cations of interest start at the anode-side microchannel where the concentration is equal to the reservoir concentration, and proceed towards the cathode. For simplicity we assume also that the valence of the analyte is the same as the valence of the cation in the BGE and that the mobility of each species in the system is constant (*e.g.*, we do not consider ionic strength or pH effects on mobility[55]). This analysis is presented in detail in Appendix II.

In Fig. 5 we provide the resulting relations from the analysis in Appendix II. The results describe the area-averaged stacking ratio of a cationic analyte species, i, between each region of the microchannel–nanochannel system and the reservoir concentration. In typical fluorescence microscopy, the area averaged stacking ratio is directly related to the measured increase in fluorescence intensity inside the channel. Therefore, the stacking ratio is the experimentally accessible quantity. Stacking ratios in each region of the microchannel–nanochannel–microchannel system are given in terms of the key system parameters: channel height ratios, nondimensional mobilities, and Dukhin number, $1/c_{0,r}^* h_n^*$. These are typically all known quantities.

The results shown in Fig. 5 indicate that a cationic analyte may be used to trace the development of the enrichment and depletion fronts. In the depletion region (first column of equations in Fig. 5), the local-to-reservoir cationic stacking ratio is inversely proportional to the nondimensional microchannel height, h_d^*. h_d^* is typically very large, therefore we expect the concentration of a cationic analyte to approach zero inside the depletion region. This is similar to the behavior of the depletion region background electrolyte concentration which also approaches zero, making cationic analytes suitable for tracking the extent of the depletion region. In the enrichment region, the cationic analyte stacking ratio (rightmost column of Fig. 5), exactly matches the increase in the background electrolyte (eqn (7) and (8)). This makes a cationic tracer suitable as to both track the extent of and measure the concentration inside the enrichment region. Finally, the cationic stacking ratio inside the nanochannel is a function of both the analyte mobility, ν_i^*, and the BGE properties. Therefore, the cationic stacking ratio is not a simple measurement of the BGE concentration inside the nanochannel.

Experimental results from Pu *et al.*[14] showing the behavior of Rhodamine 6G in a Borofloat glass device with a 60 nm deep nanochannel are shown in Fig. 6(a)–(e), below. In these experiments an electric field was applied from right to left along a nanochannel (not visible) joining the two U-shaped microchannels shown in the figure (the anode and cathode are respectively on the right and left). As predicted by the results in Fig. 5, the concentration on the cathode side of the nanochannel (where we expect the enrichment region) increases and the concentration on the anode side decreases. Furthermore, the case where fluorescein is used as an analyte

¶ The enrichment shock is the only interface in such a system where V^{int} is positive and nonzero. However, Mani *et al.*[11] and Zangle *et al.*[2] showed that this interface travels at the bulk velocity, so $U^{\text{bulk}} = V^{\text{int}}$. Therefore, the total species velocity (in this interface frame of reference) on either side of this interface will be U_i^{eph} which has the same sign on either side of the enrichment shock.

‖ Their work considers ions which move in the same (over-speeder) or opposite (counter-speeder) directions as the ITP velocity. We extend this to describe channels with variable depth and to include the effects of bulk flow on total species velocity.

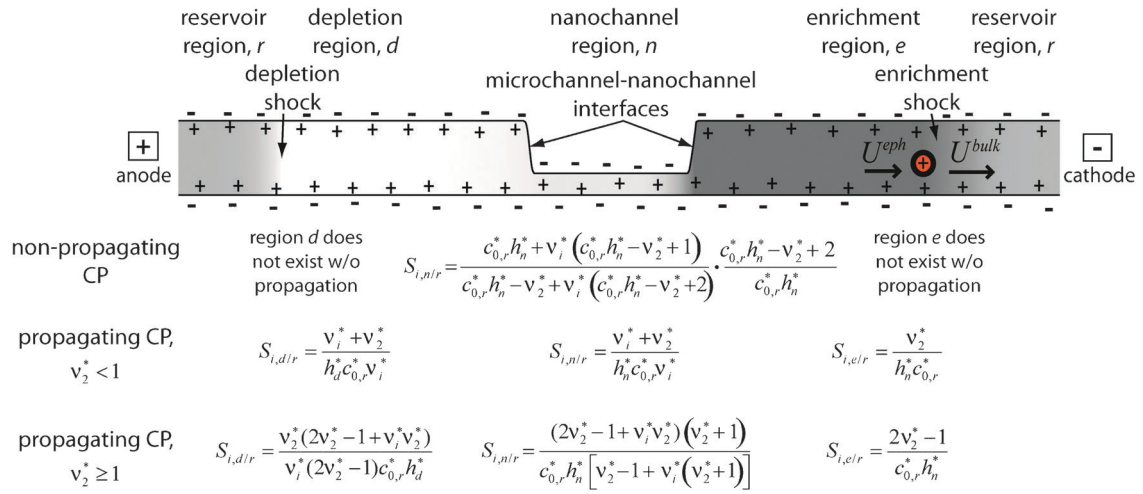

Fig. 5 Summary of results for area-averaged stacking ratios of cationic analytes from analysis in Appendix II. Results were derived by balancing cationic species flux across each of four labeled interfaces (depletion shock, microchannel–nanochannel interfaces, enrichment shock) in the system. Note that the depletion region stacking ratio, $S_{i,d/r}$, is inversely proportional to the microchannel height in the depletion region nondimensionalized by the nanoscale reference length, h_d^*. Since h_d^* is typically very large, the concentration of a cationic species will be very low in the depletion region. This makes cationic tracers suitable for tracking the boundary of the depletion region, as was observed by Pu *et al.*[14] and used in experiments by Kim *et al.*[19]

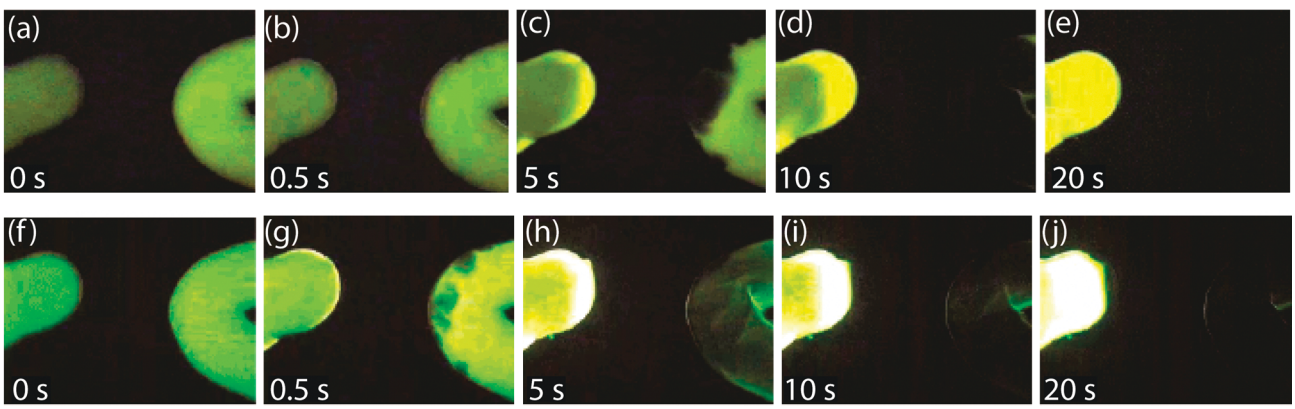

Fig. 6 Typical third species focusing behavior in a microchannel–nanochannel–microchannel experiment from Pu *et al.*[14] Images (a) through (e) show Rhodamine 6G in 100 μM phosphate buffer (reported as pH = 7) at 0 (before voltage was applied), 0.5, 5, 10 and 20 s after voltage was applied. Images (f)–(j) show behavior of fluorescein in 70 μM sodium tetraborate (with reported pH = 8) at the same times. The device consists of two U-shaped microchannels (extending out of the left and right side of each image) connected by a 60 nm deep nanochannel. Both sets of images show a strong analyte depletion zone (right side) as expected by theory. The Rhodamine 6G images of (a)–(e), show the cationic dye acting as a tracer with an increased concentration in the enrichment region, consistent with the results shown in Fig. 5. The fluorescein experiments, images (f) through (j), show either focusing at the enrichment side interface (consistent with model predictions, see strong fluorescence intensity at the interface in (g)) or stacking on the moving enrichment shock. In image (j) the enriched zone appears to have started to move left away from the interface, consistent with enrichment shock focusing. Images at later times showing a larger gap between the interface and the enriched concentration region would be consistent with this behavior. Reprinted with permission from Pu *et al.*[14] Copyright 2004 American Chemical Society.

molecule (Fig. 6(f)–(j)) shows an enriched region which may be starting to separate from the nanochannel interface, in contrast to the Rhodamine 6G enrichment region which stays attached to the interface. This is consistent with the prediction that Rhodamine 6G, as a counter-ionic analyte, should trace the BGE enrichment region. Computational model results of background electrolyte behavior show that CP creates a net-neutral enrichment region which remains attached to the cathode-side interface.[2,9,21] The observed behavior of fluorescein in these experiments is consistent with simulation results for an anionic analyte[9,21] and will be discussed in more detail below.

As per Fig. 5, the concentration of a counter-ionic dye will be very low in the depletion region, making it suitable for tracking the edge of the depletion region over time in experiments. Consistent with this, Kim *et al.*[19] used Rhodamine 6G combined with fluorescent beads to image CP-induced vortices at the boundary of the depletion region.

Experiments by Huang and Yang[24] using Rhodamine 6G as a counter-ionic tracer showed similar results to those in

Fig. 6(a)–(e) and also used a cationic dye to trace the extent of the depletion region. Additionally, Huang and Yang[24] performed numerical simulations of the flow in the depletion region using a constant zeta potential model. This model found that recirculation occurs due to a change in the degree of EDL overlap inside the depletion region, which lowers the overall bulk velocity. They found that the pattern of the edge of the depletion front imaged using Rhodamine 6G correlated with their simulated recirculation flow profile.

Experiments with nanoporous glass beads imaged using Rhodamine 6G[12] showed a large decrease in concentration inside the beads and traced the formation of a strong enrichment zone on the cathode side of the bead. In similar experiments at a different set of condition, using normalized fluorescence intensity measurements inside a nanoporous glass bead, Tallarek *et al.*[27] visualized an increase in concentration inside the nanoporous structures as well as formation of enrichment and depletion zones. Again, to our best interpretation of the experiments, each of these results is consistent with Fig. 5.

Kim *et al.*[1] performed experiments with Rhodamine 123 loaded into only one side of a nanochannel with strongly overlapped EDLs. They showed that Rhodamine 123 was able to translocate the nanochannel upon application of an electric field. This is expected for a counter-ion which will always move in the direction of the applied electric field, and so consistent with the theory presented here. Similar experiments performed with anionic fluorescent species showed that these ions were unable to pass through the nanochannel. This behavior is also consistent with our theory and will be discussed in the next section describing behavior of anionic species.

6. Focusing and stacking of anionic analytes

In this section we consider the behavior of anionic analytes in a system with concentration polarization due to a nanochannel with negatively charged walls. Here we extend the results of preliminary work we have published on this topic[10] as well as the analysis of a recent paper by Plecis *et al.*[9] Plecis *et al.* identifies four focusing regimes for anionic analytes and presents a computational model which captures phase boundaries based on surface charge, σ, and applied potential. We here start in section 6.1 by deriving results for the behavior of anionic species using the analytical theory of Mani *et al.*[11] Using an analytical model allows us to present a generalized regime map for arbitrary buffer and surface chemistry.

In sections 6.2–6.5, we compare both the analytical model based on Mani *et al.*[11] and the computational results of Plecis *et al.*[9] to published experimental results across a wide variety of conditions. We address separately each interface in a microchannel–nanochannel system with concentration polarization. Starting from the left side of Fig. 7 we will look at anionic analyte behavior on the depletion shock (section 6.2), the depletion region side microchannel–nanochannel interface (section 6.3), the enrichment region side nanochannel-microchannel interface (section 6.4) and, finally, the enrichment shock (section 6.5).

6.1 Anionic analyte theory

To predict analyte behavior, we will look at the direction of transport of analyte anions in each region of the micro-nanochannel system relative to each interface in the system. As noted earlier, there are only four possible interfaces in a microchannel–nanochannel system with CP at which the total species drift velocity, $U_i^{\mathrm{tot}} = U_i^{\mathrm{eph}}/U^{\mathrm{bulk}} - V^{\mathrm{int}}$, changes. As shown in Fig. 7 these are the depletion shock, the microchannel–nanochannel interfaces and the enrichment shock. In this section to predict focusing *versus* stacking, we will examne U_i^{tot} at each of these interfaces. Unlike cations, anions can, in the frame of reference of an interface moving at V^{int}, migrate in opposite directions into a common focusing zone; so that

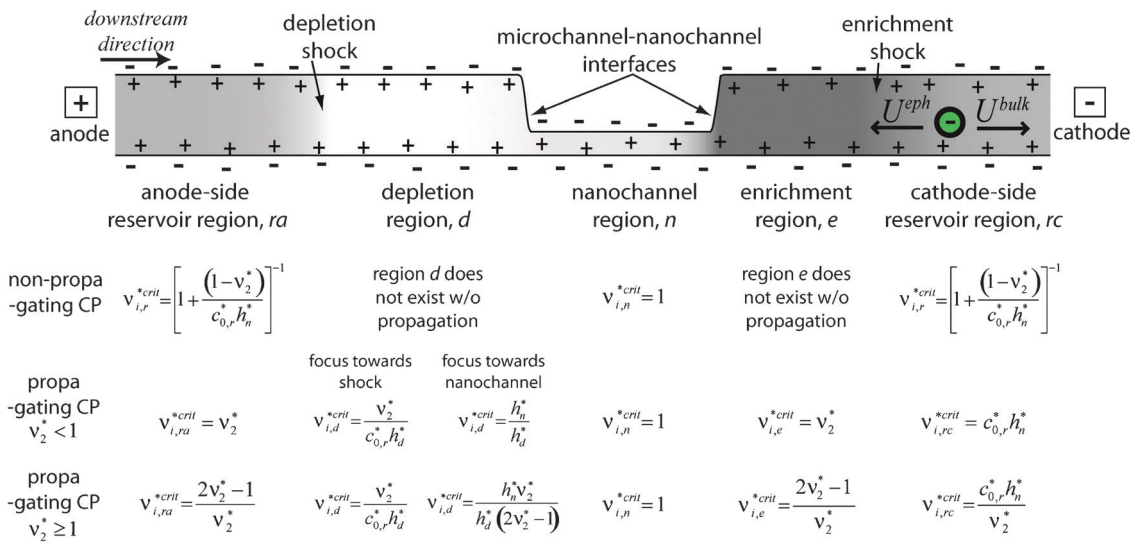

Fig. 7 Summary of results for critical values of ν_i^* for anionic analytes. For a given channel location and CP behavior (non-propagating, propagating $\nu_2^*<1$, propagating $\nu_2^* \geq 1$) if ν_i^* is greater than $\nu_i^{*\mathrm{crit}}$ then the ion will electromigrate upstream towards the anode, if ν_i^* is less than $\nu_i^{*\mathrm{crit}}$ then species i will advect downstream towards the cathode. The downstream direction (direction of bulk flow) and all four interfaces discussed in the text (depletion shock, microchannel–nanochannel interfaces, enrichment shock) are labeled in the microchannel–nanochannel schematic at the top of the figure. Details of this derivation are given in Appendix III.

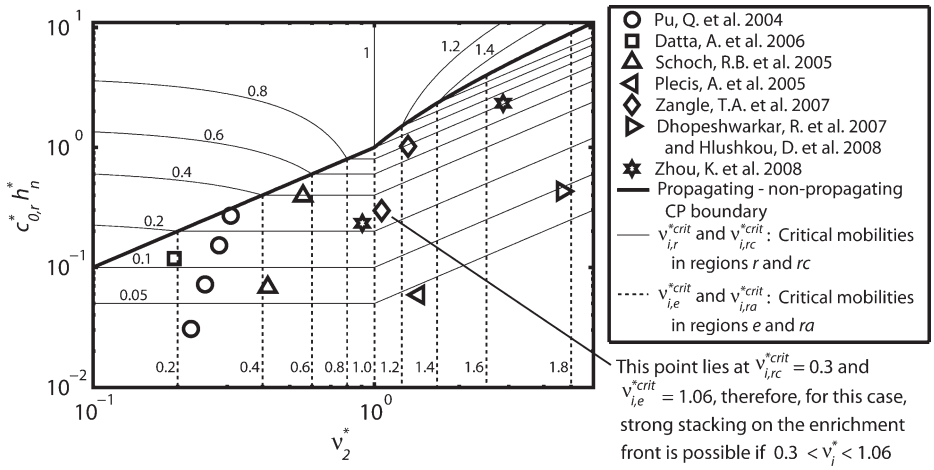

Fig. 8 Phase boundaries in the field defined by $c_{0,r}^* h_n^*$ *versus* ν_2^*. $c_{0,r}^* h_n^*$ describes the ratio of bulk conductance to surface conductance. ν_2^* describes the ratio of background electrolyte (cation) mobility to the electroosmotic mobility in the nanochannel. The dashed contours are critical values of the nondimensional mobility of negatively charged analyte species in the enrichment region ($\nu_{i,e}^{*crit}$) or in the anode side reservoir region $\nu_{i,ra}^{*crit}$. If, for example, the nondimensional analyte mobility (ν_i^*) is greater than the local $\nu_{i,e}^{*crit}$, then the analyte will electromigrate upstream in the enrichment region. The solid line contours are critical values of analyte mobility in the reservoir regions ($\nu_{i,r}^{*crit}$) for cases with no propagation, or contours of critical analyte mobility in the cathode side reservoir region ($\nu_{i,rc}^{*crit}$) for cases where CP propagates. These contours yield the mobility of an analyte which has zero total velocity in the reservoir region as a function of $c_{0,r}^* h_n^*$ and ν_2^*. The thick black line is the predicted phase boundary between propagating and non-propagating CP from eqn (5) and Fig. 4. Stacking and focusing predictions are discussed in the text below. Shown together with the theory are data from 8 studies. The predicted and observed focusing behaviors for each condition are discussed in the text and Table 2. Most of the results map as expected within our theoretical framework one exception is the experiments of Schoch *et al.*[16] where enrichment side interface focusing was reported, but we predict stacking on the enrichment side interface.

U_i^{tot}changes sign on either side of the interface.** More details of the derivation of these results is presented in Appendix III. Here, we introduce the results presented in Fig. 7 and Fig. 8. We defer detailed discussion of these results relative to experimental observations sections 6.2–6.5.

The interfaces created by the junctions of the microchannels and nanochannel have zero velocity, so that $V^{int} = 0$. Since, for a negatively charged channel system, anions electromigrate in the opposite direction of bulk flow, we will examine the ratio of the local electrophoretic velocity of the co-ionic species divided by the local bulk velocity, U_i^{eph}/U^{bulk}. Each of these velocities is here measured relative to the laboratory frame. If $U_i^{eph}/U^{bulk} > 1$, then the local electrophoretic velocity is higher than the local bulk velocity and the anionic species electromigrates upstream, against the direction of bulk flow. When $U_i^{eph}/U^{bulk} < 1$, the anionic species advects downstream in the direction of bulk flow. The ratio U_i^{eph}/U^{bulk} in each region of the system, therefore, defines the critical value of the anion mobility, ν_i^{*crit}, at which the anion's total velocity changes sign. We can then compare the non-dimensional analyte anion mobility, ν_i^*, which is assumed to be constant and uniform throughout a given system, to the computed values of ν_i^{*crit} in each region. If the analyte anion mobility, ν_i^*, is greater than the critical value, ν_i^{*crit}, downstream of a particular interface, and less than the critical value upstream of the same interface, then that analyte anion will be transported inwards towards that interface and will focus. We examine this condition in more detail in sections 6.3 and 6.4.

At the enrichment region shock, $V^{int} = U^{bulk}$.[2,11] Therefore, as presented in Appendix III, analyte anions can never focus at this interface (since U_i^{eph} cannot change sign). Experimental observations do show stacking at the enrichment shock, accompanied by a decrease in concentration in the near-nanochannel region[10,21,22] (*cf.* Fig. 10). This type of stacking is captured by the theory as regions where the critical mobility, ν_i^{*crit}, on the anode side of the enrichment shock is lower than ν_i^*, which is in turn lower than ν_i^{*crit} on the cathode side. We examine this condition in more detail in section 6.5.

At the depletion region shock V^{int} is a known function of the background electrolyte and channel properties.[11] In Appendix III we derive results for the critical nondimensional analyte mobilities, ν_i^{*crit}, at which ions will focus on the moving depletion shock. We examine focusing on the depletion shock in more detail in section 6.2.

As a preliminary note, ν_i^* is defined as the ratio of the analyte electrophoretic velocity to the bulk (electroosmotic) velocity inside the nanochannel ($\nu_i^* = (\nu_i z_i F\eta)/(\zeta_n \varepsilon)$). Therefore, inside the nanochannel, $U_{i,n}^{eph} \Big/ U_n^{bulk} = \nu_i^*$ by definition, and for all conditions:

$$\nu_{i,n}^{*crit} = 1 \qquad (9)$$

Eqn (9) means that for $\nu_i^* > 1$ ions of species i will be fast enough to travel upstream inside the nanochannel, and for $\nu_i^* < 1$, ions of species i will be too slow to beat bulk flow and so will advect downstream through the nanochannel. In other zones of the channel system (*e.g.* the enrichment zone) the critical nondimensional mobility is not necessarily unity because the background electrolyte concentration and the

** The enrichment shock is the only interface in such a system where V^{int} is positive and nonzero. However, Mani *et al.*[11] and Zangle *et al.*[2] showed that this interface travels at the bulk velocity. Therefore, the total species velocity on either side of this interface will be U_i^{eph} which has the same sign on either side of the enrichment shock.

Table 1 Definition of symbols used

Symbol	Description	Units (SI)	Symbol	Description	Units (SI)
I	Current	C s^{-1}	F	Faraday's constant	C mol^{-1}
w	Channel width	m	h	Channel height	m
z_i	Valence of species i	—	c_i	Concentration of species i	mol m^{-3}
U^{bulk}	Bulk velocity	m s^{-1}	ν_i	Mobility of species i	m mol N^{-1} s^{-1}
E	Electric field	N C^{-1}	G	Conductance per length	C^2 N^{-1} s^{-1}
c_0	Counter-ion concentration outside of EDLs	mol m^{-3}	σ	Surface charge density	C m^{-2}
η	Fluid viscosity	N s m^{-2}	λ_d	Debye length	m
ζ	Zeta potential	N m C^{-1}	e	Elementary charge	C
k	Boltzmann's constant	N m K^{-1}	T	Temperature	K
U^{eph}	Electrophoretic velocity	m s^{-1}	h_{ref}	Nanoscale reference length	m
Q	Flowrate per unit width	m^2 s^{-1}	V^{shock}	Shock velocity	m s^{-1}
ε	Solution permittivity	C^2 N^{-1} m^{-2}		Electric potential	N m C^{-1}
U_i^{tot}	Total species drift velocity	m s^{-1}	V^{int}	Velocity of an interface	m s^{-1}
r	Reservoir region subscript	—	d	Depletion region subscript	—
ra	Anode side reservoir region subscript	—	rc	Cathode side reservoir region subscript	—
e	Enrichment region subscript	—	n	Nanochannel subscript	—
1	Background electrolyte counter-ion species subscript	—	2	Background electrolyte co-ion species subscript	—
i	Analyte species i subscript	—	h_n^*	Nanochannel height normalized by nanoscale reference length	—
ν_2^*	Electrophoretic mobility of species 2 nondimensionalized by nanochannel electroosmotic mobility	—	$c_{0,r}^*$	Reservoir concentration nondimensionalized by wall charge and channel size	—
I^*	Nondimensional current	—	Pe	Peclet number based on channel height, $Pe = U^{bulk}h/D$	—
$S_{i,n/r}$	Area-averaged stacking ratio of cationic analyte i, from region n to region r	—	$f_{i,r}$	Flux of analyte species i in region r	—

electric field vary locally due to CP. For these zones the theory of Mani *et al.*[11] can be employed to predict the relative strength of the electrophoretic to bulk velocities in each region of the micro-nanochannel system. Equating this ratio to unity yields the critical mobility in each zone in terms of key system parameters (channel height ratios, Dukhin number, and non-dimensional mobility of the co-in in the BGE). We defer the details of the analysis to Appendix III and present the results of critical mobilities in each zone in Fig. 7.

We again stress that the changes in ν_i^{*crit} across each of the four interfaces in Fig. 7 indicate the existence and degree of a stacking or focusing situation due to local changes in electric fields and bulk flow velocities. For example, a decrease in the magnitude of ν_i^{*crit} from region e to rc indicates slowing of anions as they move across the enrichment shock.†† This change of velocity is due to a change in electric field which, in turn, is caused by the concentration difference across this interface. (Note that since fluid mass is conserved, the bulk flow velocities on either side of the enrichment (or depletion) region shock in a constant area microchannel are the same, so a change in ν_i^{*crit} reflects a change in local electric field.) This can lead to the case where an ion is transported downstream in one region relative to an interface (where $\nu_i^* < \nu_i^{*crit}$), and upstream in the next region relative to an interface (where $\nu_i^* > \nu_i^{*crit}$), hence focusing or stacking at the interface. Fig. 7 is therefore a general framework for predicting both stacking and focusing behavior in these systems.

The results for critical values of ν_i^* are plotted in Fig. 8. Note that the critical value of ν_i^* in the depletion region (region d) relative to either the depletion shock or the microchannel–nanochannel interface depends on the nondimensional depletion region height, h_d^*. Over the domain of $c_{0,r}^* h_n^*$ and ν_2^* represented in Fig. 8 and for the minimum reported value of h_d/h_n of 20,[2] $\nu_{i,d}^{*crit} \leq 0.05$. This critical value is lower than any computed ν_i^* based on the literature surveyed here. In practice, this means that the electric field in the depletion region is high enough that all reported anionic species travel upstream faster than the depletion shock, with both $U_i^{eph}/U^{bulk} > 1$ and $U_i^{eph}/U^{bulk} > 1 - V^{shock}/U^{bulk}$, and, therefore, we do not plot values of $\nu_{i,d}^{*crit}$ in Fig. 8. Table 1.

We illustrate the utility of Fig. 8 by considering an example case: a data point from Zangle *et al.*[10] at $c_{0,r}^* h_n^* = 0.3$ and $\nu_2^* = 1.06$: In this case, experimental conditions (including the specific background electrolyte or buffer used) determine $c_{0,r}^* h_n^*$ and ν_2^*. We plot a point at these coordinates as shown in Fig. 7. Since the point is below the thick solid line, the model predicts propagating CP with large enrichment and depletion regions (a point above the line indicates non-propagating CP). We then either compute $\nu_{i,e}^{*crit}$, $\nu_{i,rc}^{*crit}$ and $\nu_{i,ra}^{*crit}$ from the results in Fig. 7 or read their values from the $\nu_{i,e}^{*crit}$, $\nu_{i,rc}^{*crit}$ and $\nu_{i,ra}^{*crit}$ contours of Fig. 8 to establish stacking or focusing situations.

†† First, consider an analyte species with $\nu_{i,n}^*$ greater than both values of ν_i^{*crit}. Such an ion moves quickly upstream toward the interface, as ν_i^{*crit} is low in the downstream region. When this species crosses into the upstream region, it slows down, since its ν_i^* is now closer to the local ν_i^{*crit} (at $\nu_i^* = \nu_i^{*crit}$ the total species velocity would be zero). This change in total velocity from a high to low value will cause local stacking, but not focusing. Similarly, an ion advecting downstream with ν_i^* less than both values of ν_i^{*crit} will also change from high velocity to low velocity when $\nu_{i,upstream}^{*crit} > \nu_{i,downstream}^{*crit}$. Therefore, a species with very low ν_i^* will also stack under these conditions.

Table 2 Predicted and Observed Analyte Ion Behaviors. The parameters $c^*_{0,r}h^*_n$, ν^*_2 and ν^*_i are estimated based on literature data for zeta potential[48–49] and mobility[57,63–65]

Reference	$c^*_{0,r}h^*_n$	ν^*_2	ν^*_i	Predicted behavior	Observed behavior
Pu, Q. *et al.* 2004[14]	0.03	0.22	0.37	Enrichment-side interface focusing	Enrichment-side interface focusing or enrichment shock stacking
	0.07	0.25	0.42		
	0.15	0.28	0.47		
	0.27	0.31	0.52		
Datta, A. *et al.* 2006[18]	0.12	0.19	0.33	Enrichment-side interface focusing	Enrichment-side interface focusing
Schoch, R.B. *et al.* 2005[16]	0.07	0.42	0.12	Enrichment side interface stacking	Enrichment-side interface focusing
	0.39	0.56	0.16		
Plecis, A. *et al.* 2005[15]	0.06	1.43	0.72	Enrichment-side interface focusing	Enrichment-side interface focusing
Zangle, T.A. *et al.* 2007[10]	0.30	1.06	0.34	Enrichment shock stacking	Enrichment shock stacking
	0.30	1.06	0.58		
	1.02	1.32	0.79		
Dhopeshwarkar, R. *et al.* 2008[21]	0.43	4.66	1.77	Enrichment shock stacking	Enrichment shock stacking
	0.43	4.66	2.33	No stacking	
Hlushkou, D. *et al.* 2008[22]	0.43	4.66	0.59	Enrichment shock stacking	Enrichment shock stacking
Zhou, K. *et al.* 2008[26]	0.23	0.91	0.72	Depletion shock focusing	Depletion shock stacking/focusing
	2.33	2.87	1.43		

Keep in mind that the critical value of ν^*_i in the nanochannel is unity, and the critical value of ν^*_i in the depletion region is typically lower than ν^*_i for most analytes. In this example, $\nu^{*\mathrm{crit}}_{i,e} = 1.06$, $\nu^{*\mathrm{crit}}_{i,rc} = 0.3$ and $\nu^{*\mathrm{crit}}_{i,ra} = 1.06$. Next, we compute the analyte nondimensional mobility ν^*_i. In this case, we found $\nu^*_i = 0.34$ for one of the analytes studied (see Table 2). Finally, stacking or focusing is possible only if the analyte slows down as it moves through an interface. Therefore, we identify interfaces where the critical analyte mobility is higher upstream than downstream (downstream direction defined as the direction of bulk flow in the system). In this example $\nu^{*\mathrm{crit}}_{i,ra} > \nu^{*\mathrm{crit}}_{i,id}$ and $\nu^{*\mathrm{crit}}_{i,ie} > \nu^{*\mathrm{crit}}_{i,re}$, so we predict an increase in analyte concentration at both the depletion and enrichment shocks. Next, we look at how the value of ν^*_i for our analyte of interest compares to the critical values in the system. In this case $\nu^*_i < \nu^{*\mathrm{crit}}_{i,e}$ and $\nu^*_i > \nu^{*\mathrm{crit}}_{i,rc}$, therefore, this analyte is expected to stack strongly on the enrichment shock. This matches well with the experimental observation of strong enrichment shock stacking. This procedure was carried out for each of the experimental conditions in Fig. 8. The results of this analysis are summarized in Table 2 and the sections below. Appendix IV shows a supplementary figure where this example is worked out graphically.

In the following sections, we will consider possible focusing and stacking criteria at each interface shown in Fig. 7. We will also compare the model presented here (based in part on Mani *et al.*[11]) to published experimental results. This comparison is summarized in Table 2.

6.2 Depletion shock

When CP propagates, focusing of analytes at the depletion shock occurs when the analyte mobility is low enough that analytes travel in the direction of bulk flow inside the reservoir region but high enough that they travel against bulk flow in the depletion region. This condition can be written as: $\nu^{*\mathrm{crit}}_{i,d} < \nu^*_i < \nu^{*\mathrm{crit}}_{i,ra}$. For all reported cases of ν^*_i from the literature, $\nu^{*\mathrm{crit}}_{i,d} < \nu^*_i$. This is because the concentration in the depletion region is very low, therefore, the electric field is very high. The high electric field in the depletion region causes all

analytes to have a very high electrophoretic velocity here. Therefore, for all practical anions we know of in systems with typical microchannel heights ($c^*_{o,r}h^*_d \gg 1$), analyte ions will move upstream inside the depletion region (against the direction of bulk flow) faster than the depletion region shock velocity. Plecis *et al.*[9] termed this regime anode cathode gradient focusing (ACGF).

Analytes which do not meet the focusing condition can still stack on the depletion shock as long as $\nu^{*\mathrm{crit}}_{i,d} < \nu^{*\mathrm{crit}}_{i,ra}$. For all CP cases examined here, this condition is met, and stacking at the depletion shock interface should occur. Physically, this condition means that anionic analyte ions traveling towards the depletion shock through the depletion region will slow down once they reach the shock, causing an increase in concentration.

The depletion shock is a strong shock[11] and, therefore, has large changes in concentration over very short distances (see Fig. 3). These large concentration gradients in the background electrolyte create high electric field gradients. These field gradients, in turn, are very suitable for focusing of analytes to very high concentrations. We will discuss applications of focusing on a depletion shock in the last section of this review.

In an experiment[56] with the same buffer and channel conditions as Zangle *et al.*[10] we noted focusing on the depletion shock, as predicted by theory. Zhou *et al.*[26] also noted focusing on the depletion shock, as expected by theory.

6.3 Depletion side microchannel–nanochannel interface

In the previous section we showed that anions can focus on the moving boundary of the depletion shock. Next, we will examine possible anion behaviors at the depletion-side microchannel–nanochannel interface. According to the theory presented in Fig. 7 and Fig. 8, focusing or stacking at the depletion side microchannel–nanochannel interface should not be possible if CP propagates. This is because the concentration in the depletion region is very low, therefore the electric field is very high, and co-ionic species travel very quickly upstream in this region. This corresponds to very low values of $\nu^{*\mathrm{crit}}_{i,d}$ in the analytical theory outlined above. This focusing or stacking location corresponds to the anode stacking (AS) regime of Plecis *et al.*[9]

As indicated schematically in Fig. 2, in cases where CP does not propagate, focusing or stacking is possible at this interface if $\nu^{*\mathrm{crit}}_{i,n} < \nu^{*\mathrm{crit}}_{i,r}$. Focusing will occur if $\nu^{*\mathrm{crit}}_{i,n} < \nu^{*}_{i} < \nu^{*\mathrm{crit}}_{i,r}$. Stacking will occur if $\nu^{*\mathrm{crit}}_{i,n} < \nu^{*\mathrm{crit}}_{i,r}$ and ν^{*}_{i} is either larger or smaller than the critical mobilities in the nanochannel and the reservoir.

A conference paper by Plecis *et al.*[20] presents visualizations of depletion side preconcentration of an analyte. The channel layout consisted of a very wide microchannel connected to a much narrower nanochannel. The visualizations show an increase in fluorescence intensity very close to the depletion side nanochannel interface (in contrast to the model described here which predicts stacking on the depletion shock). We hypothesize that their geometry (which is difficult to analyze with our model) may result in a propagating CP case where stacking of the analyte appears to be very similar to focusing on the depletion side interface. We will analyze the effects of strong in-plane changes of channel geometry (as in this Plecis *et al.*[20] work) in a future paper. To the best of our knowledge, focusing or stacking at the depletion side interface has not been demonstrated experimentally in a device with constant (in-plane) width channels and propagating CP.

6.4 Enrichment side microchannel–nanochannel interface

In this section we consider the enrichment side microchannel–nanochannel interface. The analysis above shows that focusing or stacking can occur at this interface with either propagating or non-propagating CP. We are not aware of any observations of an increase in analyte concentration at the enrichment side nanochannel interface in non-propagating CP. Plecis *et al.*[9] termed focusing or stacking at the enrichment side nanochannel interface as cathode stacking (CS).

When CP propagates, an analyte species focuses on the enrichment side nanochannel interface if its mobility is too low to travel against bulk flow inside the nanochannel, but high enough to travel against bulk flow in the enrichment region. This condition can be written as: $\nu^{*\mathrm{crit}}_{i,e} < \nu^{*}_{i} < \nu^{*\mathrm{crit}}_{i,n}$, or, since the critical analyte nondimensional mobility inside the nanochannel is always unity, we can write the condition for focusing on the enrichment side nanochannel interface as

$$\nu^{*\mathrm{crit}}_{i,e} < \nu^{*}_{i} < 1 \tag{10}$$

For non-propagating CP there is no appreciable length of the enrichment region (any increase in background electrolyte concentration due to CP will be very localized). Therefore, we only need to consider the behavior of anions in the reservoir region. The condition for focusing at the enrichment side nanochannel interface for non-propagating CP is

$$\nu^{*\mathrm{crit}}_{i,r} < \nu^{*}_{i} < 1 \tag{11}$$

Finally, for propagating CP, stacking is possible at this interface if analyte ions have a higher electrophoretic velocity in the enrichment region than in the nanochannel. Therefore the stacking condition is

$$\nu^{*\mathrm{crit}}_{i,e} < 1 \tag{12}$$

The stacking condition for non-propagating CP is

$$\nu^{*\mathrm{crit}}_{i,r} < 1 \tag{13}$$

Pu *et al.*[14] show behavior consistent with either focusing at the enrichment side nanochannel interface or stacking at an enrichment shock. The ambiguity is because, in the last time-series images reported, the regions of increased analyte concentration appear to be moving slightly away from the microchannel–nanochannel interface, though they have not propagated very far (see Fig. 6(f)–(j)). For all reported experimental cases our model predicts focusing at the enrichment side interface. Better comparison to experiments would require longer time series data. In related work, Datta *et al.*[18] show results consistent with focusing on the enrichment side nanochannel interface and in agreement with our model.

Schoch, *et al.*[16] also report focusing at the enrichment side nanochannel interface (Fig. 9), however, for their reported conditions, our model predicts either stacking on the enrichment side nanochannel interface or stacking on a propagating enrichment shock. This discrepancy may be due to the low

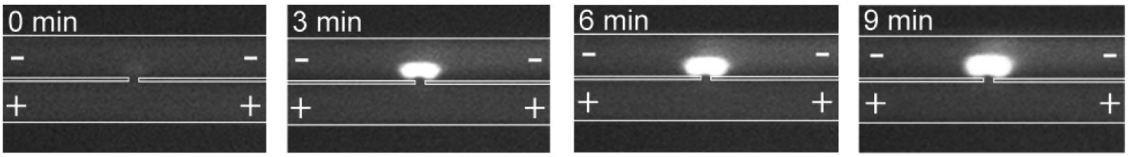

Fig. 9 Visualization of green fluorescent protein (GFP) focusing at the enrichment side nanochannel interface. The model presented here predicts that this analyte should focus on a propagating enrichment shock, not at this interface. We hypothesize the discrepancy may be due to the low field values used or to our uncertainty in GFP mobility at these conditions. Reprinted with permission from Schoch *et al.*[16]

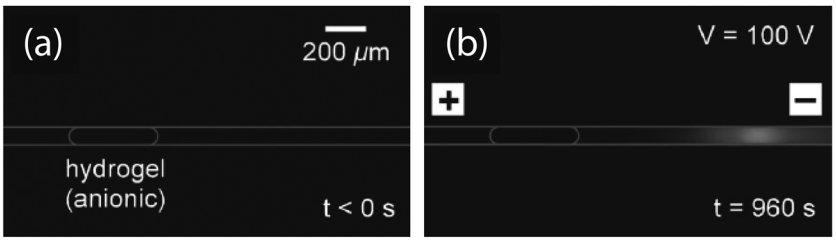

Fig. 10 Results from Hlushkou *et al.*[22] showing stacking of an anionic species on an enrichment shock. (a) shows the channel before a potential was applied. At 960 s after the voltage was applied (b), an enriched fluorescent sample zone has formed and moved away from the interface between the microchannel and the anionic, nanoporous HEMA hydrogel. These dynamics are characteristic of co-ionic species stacking on an enrichment region shock. Theory (both the theory presented here and that of Hlushkou *et al.*[22] and Dhopeshwarkar *et al.*[21]) suggests that this occurs when the fluorescent species electrophoretic velocity is equal to the bulk velocity at the CP enrichment shock (in the lab frame). Reprinted with permission from Hlushkou *et al.*[22] Copyright 2008 Royal Society of Chemistry.

applied potential in this experiment (10 V or less). A low applied electric field (and low Peclet number) may prevent the enrichment shock from propagating far enough to overcome diffusion in the vicinity of the pore. Another possible reason for this discrepancy may be our uncertainty in the mobility of GFP (we roughly estimated its mobility as 1×10^{-9} m^2 V^{-1} s^{-1}).[57] We also note that this Schoch paper discusses an increase of fluorescence concentration over time at a higher ionic strength. At this higher ionic strength, our model also predicts stacking at the enrichment side interface.

6.5 Enrichment shock

Here, we consider the final interface shown in Fig. 7, the enrichment shock. The model presented in section 6.2 predicts that anionic species can stack at the interface between the enrichment region and the reservoir region during propagating CP. This behavior is accurately described as stacking because in a frame of reference moving with the enrichment shock, the anionic total species velocity does not change its sign across the shock.[47] Physically, the enrichment shock propagates at the bulk velocity,[2,11] so in a frame moving with the enrichment shock, the only component of the species velocity is due to electrophoresis. The electrophoretic velocity is always negative, and therefore, does not cross zero at the shock front. It is possible, however, for anions to have a net inward velocity (towards the enrichment shock) in the lab frame.

When CP propagates, analytes move inwards on either side of the enrichment shock if their mobility is low enough to travel in the direction of bulk flow inside the enrichment region but high enough to travel against bulk flow in the reservoir region. This condition can be written as: $\nu_{i,rc}^{*\mathrm{crit}} < \nu_i^* < \nu_{i,e}^{*\mathrm{crit}}$. Analytes which do not meet this condition can still stack on the enrichment shock provided $\nu_{i,rc}^{*\mathrm{crit}} < \nu_{i,ie}^{*\mathrm{crit}}$. If this second condition is met, analyte ions traveling across the shock will slow down in the enrichment region, causing an increase in concentration.

Enrichment shock stacking was described analytically by Zangle *et al.*[10] and computationally by Plecis *et al.*,[9] who called this type of stacking cathodic counter gradient focusing, or CCGF. Zangle *et al.* presented results for two specific buffer cases in terms of a Dukhin number and the nondimensional mobility of the focusing species and correctly predicted the observed stacking behavior. The latter paper also presented experiments in which the enrichment region shock was used to stack and separate ions on the basis of their electrophoretic mobilities. This is possible because, in propagating CP, the enrichment shock is a weak shock[2,11] which creates an order 100 μm long[2] region with gradients in concentration and electric field. In contrast, the strong shock of the depletion region shock is typically much shorter (roughly on the order of the microchannel width), and, therefore, not typically appropriate for separation. The length of the enrichment shock is typically large compared to the ~10 μm peak widths of focused species; and so species visibly separate.[10] To date, we have not been able to (and have not seen in published work) significant separation resolution achieved using enrichment shocks. We hypothesize that the relatively low ratio of electric fields across these interfaces simply yield low peak capacity; further, preconcentration is limited to order 100×.[10,22]

Papers by Hlushkou *et al.*[22] and Dhopeshwarkar *et al.*[21] each presented an enrichment region stacking scheme along with a supporting computational model. A sample experimental result is shown in Fig. 10. As summarized in Table 2, these experimental results agreed well with the prediction of enrichment shock stacking.

7. Applications

In this section, we present several example applications of CP in devices which are tools for analysis of chemical and biological species or fluid pumping. The main application of CP has been for on-chip sample preconcentration.[58] In a 2005 paper, Wang *et al.*[17] used current through a nanochannel to create a CP depletion zone, and then focus protein on the boundary between the depletion zone and a region of the microchannel at the reservoir concentration. This technique requires that the preconcentrator use a different geometry than the serial microchannel–nanochannel–microchannel geometry considered here. The Wang *et al.*[17] device has two independently-controlled, anode-side channels so that an electroosmotic flow can be directed perpendicular to the axis of the nanopore. We hypothesize that, with this geometry, the depletion shock can be immobilized by adjusting the ratio of current across the two anode side channels (which controls bulk flow rate) to the current through the nanochannel (which controls the depletion region shock velocity). The Wang study reported 10^6–10^8 fold increase in concentration of a target protein, GFP (although we believe that at least the higher preconcentration value is an overestimate). In a similar study at University of Michigan, Kim *et al.*[1] used irreversible PDMS-glass bonding as a different method to create charged nanofluidic slits and reported 10^3–10^6-fold increase in fluorescence intensity.

Since the first demonstration of basic microfluidic–nanofluidic CP preconcentrators, there have been a number of other applications of CP-based sample preconcentrators.[1,3,5,17,59,60] For example, Wang *et al.*[5] reported increased range and 500-fold improvement in sensitivity of immuno detection using immobilized, antibody labeled beads. In that study, the authors immobilized labeled beads and stopped the depletion shock at the same location inside the anode-side microchannel, as shown in Fig. 11(a). The device then preconcentrated antigens using focusing on the strong electric field gradients of the depletion shock, which increased the rate of binding to antibody labeled beads.

Kim *et al.*[25] used vortices generated at a microchannel–nanochannel interface to create a mixing device. This device consisted of a set of parallel nanochannels connected to a U-shaped microchannel and is shown in Fig. 11(b). Here, the strong electric field gradients at the depletion shock boundary are used to create strong vortices which mix the two fluid streams.

Finally, the nonlinear behavior of electroosmotic flow in the depletion region can be used to create an induced zeta potential which is proportional to the applied electric field, a phenomena called non-equilibrium electroosmosis, or electroosmosis of the second kind.[44] In flows of this kind, the total fluid velocity is proportional to electric field squared. This is in contrast to equilibrium electroosmosis where zeta potential is static and fluid velocity is directly proportional to the applied electric field. This has lead to work on using CP effects to pump fluids. In particular, in a device using nonequilibrium EOF Kim *et al.*[8] report a 5-fold increase in volumetric flow rate relative to a similar device using equilibrium electroosmosis.

8. Summary

We presented a summary of current theory describing the regimes and dynamics associated with CP in systems with microchannel–nanochannel interfaces. We summarized results from 56 sets of published experiments and found good agreement to published theory in delineating the regimes which separate propagating *versus* non-propagating CP. This comparison shows that the parameters which govern CP in a microchannel–nanochannel system are an inverse Dukhin number and the ratio of background electrolyte cation mobility to the electroosmotic mobility inside the nanochannel.

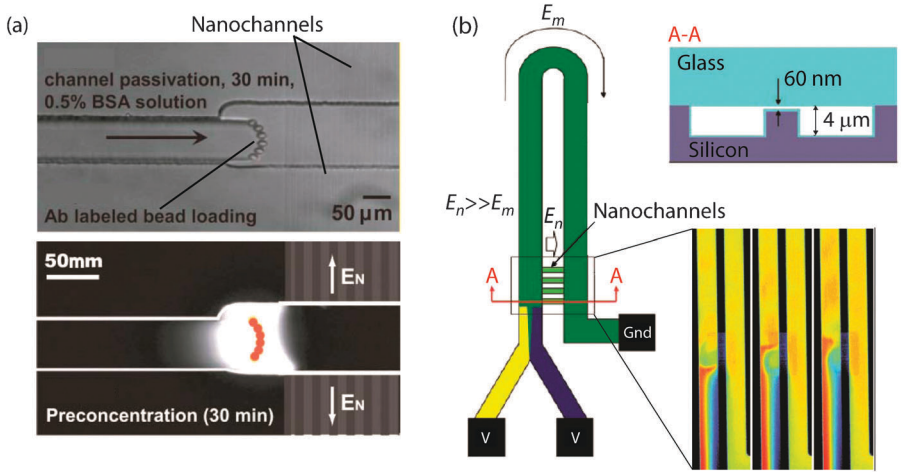

Fig. 11 Selected applications. (a) Nanofluidic preconcentrator used to increase sensitivity and dynamic range of a bead-based immunoassay.[5] Antibody-labeled beads are loaded into the microchannel and held in place adjacent to the anode side of the nanochannels used for preconcentration (top image). When an electric field is applied, a zone of focused analyte forms on top of the immobilized beads, increasing the antibody-antigen binding rate. (b) CP-based mixing device.[25] When an electric field is applied from the sample wells (at bottom, labeled with voltage, V) to the outlet well (labeled Gnd) the high electric field across the nanochannel creates a strong depletion region. Instability at the boundary of this depletion region mixes the two sample streams as shown in the images taken approximately 150 ms apart in the inset (bottom right). Adapted with permission from Wang *et al.*[5] and Kim *et al.*[25] Copyright 2008 Royal Society of Chemistry.

We then used the results of Mani *et al.*[11] to predict the behavior of cationic and anionic analytes in a microchannel–nanochannel system with negative wall charge. This included an extension of this theory to predict the conditions required for focusing or stacking of analytes in systems with CP. We predict stacking and/or focusing at four interfaces which can occur in a microchannel–nanochannel–microchannel system. We presented a comparison of this theory to published experimental data. Again we found good agreement between the reported cases from literature and the extension of the published analytical theory of Mani *et al.*[11] and Zangle *et al.*[2] presented here which predicts the existence and location of stacking and/or focusing regions.

Overall, the theory we summarize and validate in view of experimental data can be used to understand and interpret the effects of CP on analyte transport in systems containing both micro- and nanochannels.

9.1 Appendix I. Derivation of convective current through a nanochannel

In this appendix we derive a simple expression for convective current due to charge transport by electroosmotic flow through a thin channel. While a more general derivation is presented in Levine *et al.*,[61] we here consider an extreme case in which ions associated with the EDL are the only ions in the channel and the channel is very thin ($Fhzc_0/\sigma \ll 1$). Under these conditions the wall-shielding charge will have a uniform concentration equal to: $c = -2\sigma/zFh$. The solution to the Poisson–Boltzmann equation will yield the following parabolic potential:

$$\psi - \zeta = \frac{-\sigma}{\varepsilon h} y(h - y) \tag{14}$$

From eqn (1) the convective current is:

$$I_{\text{conv}} = w \int_0^h FzcU^{\text{bulk}} \mathrm{d}y \tag{15}$$

where, from Levine *et al.*[61] $U^{\text{bulk}} = \varepsilon E(\psi - \zeta)/\eta$. Substituting expressions for c and U^{bulk} and using eqn (14) yields

$$I_{\text{conv}} = \frac{wh\sigma^2 E}{3\eta}. \tag{16}$$

9.2 Appendix II. Derivation of stacking ratio for cationic analytes

As shown in Fig. 5, the microchannel–nanochannel–microchannel system can in general be divided into the following five distinct zones: 1. the undisturbed left-side microchannel, with the same concentration as in the reservoir; 2. the depletion region (if CP propagates); 3. the nanochannel; 4. the enrichment zone (if CP propagates), and 5. the undisturbed right-side microchannel. These five zones are separated by four boundaries which present possible interfaces for stacking or focusing of a cationic analyte. We assume that the cationic analyte is released from the anode-side reservoir into the channel system. In addition, we assume that the analyte is released after the nanochannel establishes its equilibrium condition. Furthermore, we consider low concentration cationic analytes compared to the background electrolyte (BGE), so that it cannot affect the axial electric field. Also, in this derivation and the anionic analyte derivation in Appendix III, following the analysis of Mani *et al.*[11] we will assume high PeL/h (*i.e.*, high product of Peclet number based on channel height and the ratio of channel length to nanochannel height) and so will not present results as a function of the applied potential or electric field.

We first present the results of the simple theory of Mani *et al.*[11] for the BGE, which determines translocation regimes in the system. Then we use their theory as a foundation to describe the effects of CP on low concentration cationic analytes.

The simplest model presented by Mani *et al.*[11] suggests that the bulk concentration of binary electrolyte in a channel system satisfies the following one-dimensional differential equation:

$$\frac{\partial}{\partial t^*}(h^* c_0^*) + \frac{\partial}{\partial x^*}\left(c_0^* + \frac{I^*}{h^* c_0^* + 1}\right) = \frac{1}{Pe}\frac{\partial}{\partial x^*}\left(h^* \frac{\partial c_0^*}{\partial x^*}\right) \tag{17}$$

where h^* is the height of the channel, non-dimensionalized by a nanoscale reference height, h_{ref}. c^* is the nondimensional bulk concentration using the wall surface-charge density, σ, which is assumed to be constant and uniform in this model:

$$c_0^* = \frac{\nu_1 z_1 - \nu_2 z_2}{2\nu_1 z_1} \frac{Fz_1 h_{\text{ref}} c_0}{-\sigma}. \tag{18}$$

With this notation, $c_0^* h^*$ is the local inverse Dukhin number. I^* is the nondimensional current through the system relative to the bulk flow rate:

$$I^* = \frac{\nu_2 z_2}{2\nu_1 z_1} \frac{Ih_{\text{ref}}}{\sigma Q}, \tag{19}$$

where Q is the bulk flow rate. The axial coordinate and time are nondimensionalized by h_{ref} and $h_{\text{ref}}^2/\text{Q}$, respectively.

Eqn (17) is a nonlinear advection-diffusion equation for evolution of the BGE, c_0^*. The nondimensional advection flux has two terms: c_0^* which represents linear advection by the bulk flow rate, and $I^*/(h^* c_0^* + 1)$ which represents exchanges between the bulk and EDL. The axial electric field in the system is the ratio of the current and local conductivity:

$$E = \frac{I}{Fz_1[F(\nu_1 z_1 - \nu_2 z_2)hc_0 - 2\nu_1 \sigma]}. \tag{20}$$

The total conductivity appeared in the denominator of eqn (20) consists of bulk effects of co- and counter-ions and the EDL conductivity. Note that c_0 is the bulk concentration of counter-ions in the BGE. From net neutrality, the bulk concentration of co-ion would be $z_1 c_0/|z_2|$, which would lead to the expression in the denominator of eqn (20) for conductivity.

An analyte ion with mobility ν_i and valence number of z_i would experience an electromigration velocity equal to $\nu_i z_i FE$. Using eqn (20) and the nondimensionalization procedure from Mani *et al.*[11] we arrive at the following expression for nondimensional electromigration velocity of the analyte:

$$\frac{\text{electromigration velocity}}{\text{bulk velocity}} = \frac{\nu_i z_i FEh}{Q} = \frac{\nu_i z_i}{-\nu_2 z_2}\frac{h^* I^*}{h^* c_0^* + 1}. \quad (21)$$

In the system considered here, the current and flow rate are not independent of each other. The current drives the electroosmotic flow through the system and the internal pressure gradients created at the microchannel–nanochannel interfaces adjust the flowrate in accordance with mass conservation. Since the nanochannel has the dominant hydraulic resistance, one can assume that the electroosmotic flow in the nanochannel determines the flow rate of the entire system. Using this assumption Mani *et al.*[11] showed that:

$$I^* = \frac{\nu_2^*}{h_n^*}(h_n^* c_{0,n}^* + 1). \quad (22)$$

As described earlier, ν_2^* is the nondimensional mobility of coions to the wall charge. It is with the assumption of eqn (22) that the entire BGE system can be parameterized by two parameters, ν_2^* and inverse Dukhin number in the nanochannel, $c_{0,r}^* h_n^*$. Substituting eqn (22) into eqn (21) yields:

$$\frac{\nu_i z_i FEh}{Q} = \nu_i^* \frac{h^*(h_n^* c_{0,n}^* + 1)}{h_n^*(h^* c_0^* + 1)}, \quad (23)$$

where ν_i^* is the nondimensional mobility of the analyte specie. Eqn (23) can be used to determine the global translocation of ions at each zone in the channel system. In this appendix, we use this equation to analyze stacking of cationic analytes for different CP regimes.

9.2.1 Non-propagating CP

If CP does not propagate, the channel system will present three zones as shown in Fig. 2c: 1. the left-side microchannel, with uniform concentration the same as concentration in the reservoir; 2. the nanochannel; and 3. the right-side microchannel with uniform concentration the same as in the reservoir. Stacking is possible at either of the two interfaces between the microchannels and the nanochannel. For this case, the equilibrium BGE concentration in the nanochannel would be lower than the reservoir's concentration due to significant flux carried by the EDL[11]

$$c_{0,n}^* = c_{0,r}^* - \frac{\nu_2^*}{h_n^*} \quad (24)$$

If one releases a cation analyte specie, i, into the left reservoir with concentration $c_{i,r}$, the analyte will travel through the left-side microchannel. Ignoring the EDL effects (in this microchannel with $c_{0,r}^* h_r^* \gg 1$), the flux of the analyte in the left-side-microchannel is:

$$f_{i,r} = c_{i,r}\,(Q + \nu_i z_i FE_r h_r) \quad (25)$$

In general, the concentration of the analyte in the nanochannel, $c_{i,n}$ would be different from its concentration in the microchannels. The flux of the analyte in the nanochannel can be written as:

$$f_{i,n} = c_{i,n}\,(Q + \nu_i z_i FE_n h_n) + f_{i,n}^{\mathrm{EDL}} \quad (26)$$

where $f_{i,n}^{\mathrm{EDL}}$ is the flux of species i in the nanochannel (region n) through the EDL. We note that $c_{i,n}$ represents only the bulk concentration of the analyte; therefore, to account for the total flux, the EDL contribution should be added. To estimate the portion of the analyte in the EDL here we assume that the analyte is distributed between the bulk and the EDL with the same proportion as in the cationic BGE. This assumption is only valid when the analyte has the same valence number as the cation in the BGE and thus satisfies the same Boltzmann distribution in the wall-normal direction:

$$\frac{\int_0^h c_i^{\mathrm{EDL}}\mathrm{d}y}{c_i^{\mathrm{Bulk}}h} = \frac{\int_0^h c_0^{\mathrm{EDL}}\mathrm{d}y}{c_0^{\mathrm{Bulk}}h} = \frac{-2\sigma/Fz_1}{c_0 h} \quad (27)$$

The second equality in eqn (27) is consistent with the simple theory of Mani *et al.*,[11] assuming that only the excess concentration of cations contributes to formation of the EDLs. Following the nondimensionalization procedure of Mani *et al.*,[11] the right-hand-side of eqn (27) can be written in terms of nondimensional quantities as:

$$\frac{\int_0^h c_i^{\mathrm{EDL}}dy}{c_i^{\mathrm{Bulk}}h} = \left(\frac{1 - \nu_2 z_2/\nu_1 z_1}{c_0^* h^*}\right) \quad (28)$$

To simplify the algebraic manipulations, in the next steps we here assume that the BGE is a symmetric electrolyte (*i.e.*, mobility and valence for the anionic BGE species equal the mobility and valence for the cationic BGE species. With this simplification, the numerator of eqn (28) reduces to a value of 2 and we arrive at a simple expression for the EDL to bulk contribution of analyte cations in terms Dukhin number based on the BGE concentration:

$$\frac{\int_0^h c_i^{\mathrm{EDL}}\mathrm{d}y}{c_i^{\mathrm{Bulk}}h} = \frac{2}{c_0^* h^*} \quad (29)$$

Using this expression we can write the EDL flux in eqn (26) as a simple correction to the bulk flux.

$$f_{i,n} = c_{i,n}[Q + \nu_i z_i FE_n h_n(1 + 2/c_{0,n}^* h_n^*)] \quad (30)$$

We note that consistent to the simple model of Mani *et al.*[11] we here assumed that ions in the EDLs are only transported *via* electromigration. The correction factor, $(1 + 2/c_{0,n}^* h_n^*)$ is simply the total to bulk concentration ratio for counterions. Due to conservation of conterionic analyte i, the flux of the analyte in the microchannel is equal to that in the nanochannel. By equating the expressions in eqn (25) and (30) one can obtain an expression for the stacking ratio of the analyte:

$$\frac{c_{i,n}}{c_{i,r}} = \frac{Q + \nu_i z_i FE_r h_r}{Q + \nu_i z_i FE_n h_n(1 + 2/c_{0,n}^* h_n^*)} \quad (31)$$

With this form stacking ratio is defined in terms of analyte concentrations in the bulk. A more useful quantity, however, is the stacking ratio in terms of the cross-sectional area-averaged concentrations (height-averaged concentrations in this case). This requires us to include the EDL contribution in the definition of stacking ratio. In our notation we use $S_{i,n/r}$ to refer to the area-averaged stacking ratio from region r to region n for analyte specie i.

$$S_{i,n/r} \equiv \frac{c_{i,n}(1+2/c^*_{0,n}h^*_n)}{c_{i,r}} = \frac{1+\nu_i z_i F E_r h_r/Q}{1/(1+2/c^*_{0,n}h^*_n)+\nu_i z_i F E_n h_n/Q} \tag{32}$$

In the next step we can write the stacking ratio in terms of system parameters, $c^*_{0,r}h^*_n$, ν^*_2, and ν^*_i. This can be simple done by substituting eqn (23) into (32) and then substituting eqn (24) into the resulting expression. Ignoring the EDL contribution of the microchannel, when evaluating eqn (23) for region r (ie. ignoring 1 relative to $h^*_r c^*_{i,r}$) leads to the following expression for $S_{i,n/r}$:

$$S_{i,n/r} = \frac{c^*_{0,r}h^*_n + \nu^*_i(c^*_{0,r}h^*_n - \nu^*_2 + 1)}{c^*_{0,r}h^*_n - \nu^*_2 + \nu^*_i(c^*_{0,r}h^*_n - \nu^*_2 + 2)} \frac{c^*_{0,r}h^*_n - \nu^*_2 + 2}{c^*_{0,r}h^*_n} \tag{33}$$

It will be useful to write this expression in terms of the stacking ratio of the background electrolyte, $S_{0,n/r}$ (here in terms of background cations). Having $S_{0,n/r} = (1+2/c^*_{0,n}h^*_n)c_{0,n}/c_{0,r}$ (see definition in eqn (32), eqn (33) can be written in the following form:

$$S_{i,n/r} = S_{0,n/r}\frac{1-\nu^*_i/c^*_{0,r}h^*_n + \nu^*_i S_{0,n/r}}{1-\nu^*_2/c^*_{0,r}h^*_n + \nu^*_i S_{0,n/r}} \tag{34}$$

where $S_{0,n/r}$ is equal to $(c^*_{0,r}h^*_n - \nu^*_2 + 2)/(c^*_{0,r}h^*_n)$. We note that since this expression is for non-propagating CP the denominator of eqn (34) will never equal zero. Also, eqn (34) indicates that if the analyte is slower than the BGE ($\nu^*_i < \nu^*_2$) then the stacking ration of the analyte will be higher than the stacking ratio of the background electrolyte cation.

9.2.2 Propagating CP, $\nu^*_2 \geq 1$

For this case we will start by computing the stacking ratio across the depletion front. We consider a control volume around the depletion shock moving with the shock velocity. The flux of analyte species from region r into this control volume is:

$$f_{i,r} = c_{i,r}(Q - V^{\text{shock}}h_r + \nu_i z_i F E_r h_r) \tag{35}$$

The depletion shock velocity given by the theory of Mani *et al.* is equal to

$$\frac{V^{\text{shock}}h_r}{Q} = 1 - \frac{2\nu^*_2 - 1}{c^*_{0,r}h^*_n} \tag{36}$$

The flux of analyte species from the control volume into the depletion zone can be written in a similar fashion. However, note that since the bulk concentration is very low in the depletion zone, the EDL contribution is not negligible in this zone and should be considered in the expression for the flux. Following a similar method that lead to eqn (30), we can write:

$$f_{i,d} = c_{i,d}[Q - V^{\text{shock}}h_d + \nu_i z_i F E_d h_d(1+2/c^*_{0,d}h^*_d)] \tag{37}$$

Since the background electrolyte has a very low concentration in the depletion region, current conservation demands an extremely high electric field in this region. Therefore the flux associated with the electric field has the dominant contribution in the flux term and thus, $f_{i,d}$ can be approximated as:

$$f_{i,d} \simeq c_{i,d}\nu_i z_i F E_d h_d(1+2/c^*_{0,d}h^*_d) \tag{38}$$

By equating the flux expressions in eqn (38) and (35) and using eqn (36), one can obtain an expression for the stacking ratio from the reservoir to the depletion zone:

$$\begin{aligned} S_{i,d/r} &\equiv \frac{c_{i,d}}{c_{i,r}}(1+2/c^*_{0,d}h^*_d) \\ &= \frac{\dfrac{2\nu^*_2-1}{c^*_{0,r}h^*_n} + \nu^*_i\dfrac{h^*_r(c^*_{0,n}h^*_n+1)}{h^*_n(c^*_{0,r}h^*_r+1)}}{\nu^*_i\dfrac{h^*_d(c^*_{0,n}h^*_n+1)}{h^*_n(c^*_{0,d}h^*_d+1)}} \end{aligned} \tag{39}$$

Here, we used eqn (23) to express the ratios of electromigration fluxes to the advective flux. Mani *et al.*[11] found the following expressions for the BGE concentrations in the depletion zone and the nanochannel:

$$c^*_{0,d}h^*_d = \frac{(\nu^*_2-1)^2}{2\nu^*_2-1},\ c^*_{0,n}h^*_n = \nu^*_2 - 1 \tag{40}$$

Using these expressions in eqn (39) and noting $c^*_{0,r}h^*_r \gg 1$ for a typical microchannel leads to

$$S_{i,d/r} = \frac{\nu^*_2(2\nu^*_2 - 1 + \nu^*_i\nu^*_2)}{\nu^*_i(2\nu^*_2-1)c^*_{0,r}h^*_d} \tag{41}$$

Rewriting this equation in terms of stacking ratio of the BGE leads to

$$S_{i,d/r} = S_{0,d/r}\left(\frac{\nu^*_2}{\nu^*_i}\right)\frac{2\nu^*_2 - 1 + \nu^*_i\nu^*_2}{2\nu^*_2 - 1 + \nu^{*2}_2} \tag{42}$$

which is a monotonically decreasing function of ν^*_i.

Next, we derive an expression for the stacking between the depletion zone and the nanochannel. Since the electromigration flux is the dominant term in the depletion zone, eqn (38) is still a good approximation for the flux in the depletion zone (although this equation was originally derived for a moving control surface). The flux in the nanochannel is already derived in eqn (30) except here the value of the nanochannel concentration should be replaced from eqn (40).

$$S_{i,n/d} \equiv \frac{c_{i,n}(1+2/c^*_{0,n}h^*_n)}{c_{i,d}(1+2/c^*_{0,d}h^*_d)} = \frac{\nu_i z_i F E_d h_d}{Q/(1+2/c^*_{0,n}h^*_n) + \nu_i z_i F E_n h_n} \tag{43}$$

Using eqn (23) and (40) into eqn (43) leads to

$$S_{i,n/d} = \frac{h_d}{h_n}\left(\frac{\nu_i^*}{\nu_2^*}\right)\frac{(\nu_2^*+1)(2\nu_2^*-1)}{\nu_2^*-1+\nu_i^*(\nu_2^*+1)} \quad (44)$$

Rewriting this equation in terms of stacking ratio of the BGE leads to

$$S_{i,n/d} = S_{0,n/d}\left(\frac{\nu_i^*}{\nu_2^*}\right)\frac{\nu_2^*-1+\nu_2^*(\nu_2^*+1)}{\nu_2^*-1+\nu_i^*(\nu_2^*+1)} \quad (45)$$

We can obtain a direct stacking ratio from the reservoir to the nanochannel by multiplying the expressions in eqn (45) and (42):

$$S_{i,n/r} = S_{0,n/r}\frac{2\nu_2^*-1+\nu_i^*\nu_2^*}{\nu_i^*+\nu_2^*-1+\nu_i^*\nu_2^*} \quad (46)$$

We can also write the stacking ratio from the reservoir to the nanochannel without relating it to the BGE concentration as:

$$S_{i,n/r} = \frac{(2\nu_2^*-1+\nu_i^*\nu_2^*)(\nu_2^*+1)}{c_{0,r}^*h_n^*[\nu_2^*-1+\nu_i^*(\nu_2^*+1)]} \quad (47)$$

Next, we derive an expression for the stacking ratio from the nanochannel to the enrichment zone. In the enrichment zone the EDL contribution to the flux can be neglected and the total flux can be written as:

$$f_{i,e} = c_{i,e}\,(Q + \nu_i z_i F E_e h_e) \quad (48)$$

Equating this flux to the flux associated with the nanochannel leads to an expression for the stacking ratio from nanochannel to the enrichment zone:

$$S_{i,e/n} = \frac{\frac{1}{1+2/c_{0,n}^*h_n^*}+\nu_i^*}{1+\nu_i^*\frac{h_e^*(c_{0,n}^*h_n^*+1)}{h_n^*(c_{0,e}^*h_e^*+1)}} \quad (49)$$

Here, we used eqn (23) to express the ratios of electromigration fluxes to the advective flux. From Mani *et al.*[11] the BGE concentration in the enrichment zone for this case is:

$$c_{0,e}^*h_n^* = 2\nu_2^* - 1 \quad (50)$$

Using this expression together with eqn (40) in eqn (49) and noting $c_{0,e}^*h_e^* \gg 1$ for typical microchannels leads to:

$$S_{i,e/n} = \left(\frac{2\nu_2^*-1}{\nu_2^*+1}\right)\frac{\nu_2^*-1+\nu_i^*(\nu_2^*+1)}{2\nu_2^*-1+\nu_i^*\nu_2^*} \quad (51)$$

Rewriting eqn (51) in terms of the BGE stacking ratio leads to:

$$S_{i,e/n} = S_{0,e/n}\frac{\nu_i^*+\nu_2^*-1+\nu_i^*\nu_2^*}{2\nu_2^*-1+\nu_i^*\nu_2^*} \quad (52)$$

By combining eqn (52) and (46) one can see:

$$S_{i,e/r} = S_{0,e/r} \quad (53)$$

We can also write:

$$S_{i,e/r} = \frac{2\nu_2^*-1}{c_{0,r}^*h_n^*} \quad (54)$$

Finally we show that the concentration of the analyte in the cathode-side *r* region is the same as that in the anode-side *r* region. Here, we will temporarily use subscript *rc* for the cathode-side microchannel to distinguish it from the anode-side zone. We consider a control volume moving with the enrichment front and write the flux balance equation between the two sides of the front. Mani *et al.*[11] and Zangle *et al.*[2] showed that the enrichment shock advects at the bulk velocity. Furthermore, EDL contribution to the flux terms is negligible on either sides of the enrichment shock. Therefore, the only term contributing to the flux through the control surfaces is the electromigration of the bulk concentration, henceforth the flux balance equation leads to:

$$S_{i,rc/e} = \frac{c_{i,rc}}{c_{i,e}} = \frac{\nu_i z_i F E_e h_e}{\nu_i z_i F E_{rc} h_{rc}} = \frac{E_e}{E_{rc}} = \frac{c_{0,rc}}{c_{0,e}} = S_{0,rc/e} \quad (55)$$

Combining eqn (53) and (55) leads to:

$$S_{i,rc/r} = S_{0,rc/r} = 1 \quad (56)$$

The second equality is due to the fact that the anode-side reservoir has the same BGE concentration as in the cathode-side reservoir.

9.2.3 Propagating CP, $\nu_2^* < 1$

The procedure of solving the problem in this case is exactly the same as what we presented in section 9.2.2. The only difference is that the BGE concentrations are different in this case and the following values from solution by Mani *et al.*[11] should be substituted into the expressions:

$$c_{0,d}^* = c_{0,n}^* = 0,\ c_{0,e}^*h_n^* = \nu_2^* \quad (57)$$

For this case the depletion region shock velocity is given by:[11]

$$\frac{V^{\text{shock}}h_r}{Q} = 1 - \frac{\nu_2^*}{c_{0,r}^*h_n^*} \quad (58)$$

In this case in regions *d* and *n* the only term contributing to the fluxes is the EDL transport and the bulk term is zero. We avoid repeating the algebraic procedures here and only present the results of the analysis.

$$S_{i,d/r} = \frac{\nu_i^*+\nu_2^*}{h_d^*c_{0,r}^*\nu_i^*} = S_{0,d/r}\frac{\nu_i^*+\nu_2^*}{2\nu_i^*} \quad (59)$$

For the depletion region we obtain:

$$S_{i,n/d} = \frac{h_d}{h_n} = S_{0,n/d} \quad (60)$$

and combining eqn (60) and (59):

$$S_{i,n/r} = \frac{\nu_i^*+\nu_2^*}{h_n^*c_{0,r}^*\nu_i^*} \quad (61)$$

Finally, for the enrichment region

$$S_{i,e/n} = \frac{\nu_i^*\nu_2^*}{\nu_i^*+\nu_2^*} = S_{0,e/n}\frac{2\nu_i^*}{\nu_i^*+\nu_2^*} \quad (62)$$

where, using eqn (61), we obtain:

$$S_{i,e/r} = \frac{\nu_2^*}{h_n^*c_{0,r}^*} \quad (63)$$

9.3 Appendix III. analysis of focusing for anionic analytes

The objective of this appendix is to derive expressions for the critical mobility of anionic analytes in a microchannel–nanochannel–microchannel system with CP. If an analyte's mobility is higher than the local critical value, it will travel against the flow direction, whereas sub-critical analytes will have net transport in the same direction as the flow. Focusing is possible in regions where the analyte velocity field is convergent. In other words, focusing is possible where the analyte is super-critical downstream of the focusing zone and sub-critical upstream. Therefore, knowing critical mobilities at different zones of the channel system allows us to identify possible focusing zones.

It should be noted that the analysis of anion transport is less complex compared to that for cations since anions are mostly transported through the bulk and have a relatively low concentration in the EDLs. Therefore, for the purposes of this analysis, we will assume that an anionic analyte, i, is transported due to electromigration in the bulk in one direction and advection due to bulk flow in the opposite direction. The ratio of the electromigration velocity to the bulk flow velocity is, therefore:

$$\frac{U_i^{\text{eph}}}{U^{\text{bulk}}} = \frac{v_i z_i F E h}{Q} \tag{64}$$

In Appendix II we derived an expression for this ratio in the nondimensional form. Using eqn (23) in eqn (64) we have:

$$\left|\frac{U_i^{\text{eph}}}{U^{\text{bulk}}}\right| = \nu_i^* \frac{h^*(c_{0,n}^* h_n^* + 1)}{h_n^*(c_0^* h^* + 1)} \tag{65}$$

where ν_i^* is nondimensionalized such that it is always positive ($\nu_i^* = |\nu_i z_i F \mu / \varepsilon \zeta_n|$). At either side of a stationary interface in the channel system, the critical analyte mobility can be computed by equating the right-hand side of eqn (65) to unity:

$$\nu_i^{*\text{crit}} = \frac{h_n^*(c_0^* h^* + 1)}{h^*(c_{0,n}^* h_n^* + 1)} \tag{66}$$

As discussed earlier, focusing will occur at a moving interface when the total species velocity in a frame moving with the interface, $U_i^{\text{eph}}/U^{\text{bulk}} - V^{\text{int}}$, changes sign. Therefore, at a moving interface, the critical analyte mobility can be computed by equating the right hand side of eqn (65) to one minus the interface velocity normalized by the bulk velocity:

$$\nu_i^{*\text{crit}} = \left(1 - \frac{V^{\text{int}}}{U^{\text{bulk}}}\right) \frac{h_n^*(c_0^* h^* + 1)}{h^*(c_{0,n}^* h_n^* + 1)} \tag{67}$$

Note, however, that the enrichment shock velocity is equal to the bulk velocity[2,11] so at this interface analyte anions can never focus (on both sides of this interface, $\nu_i^* > \nu_i^{*\text{crit}}$, and so the analyte anion total velocity can never change sign). However, experimental observations have shown that, under some conditions anionic species can be transported inwards towards the enrichment shock in the lab frame.[21,22,9,10] Therefore, on either side of the enrichment shock we will look at the total species velocity in the lab frame and define $\nu_i^{*\text{crit}}$ using eqn (66).

For different CP regimes, Mani *et al.*[11] derived expressions for concentration in the five zones of the channel system. The task of this appendix is to substitute these expressions into eqn (66) and (67) and obtain closed form expressions for critical mobility in terms of known system parameters.

9.3.1 Non-propagating CP

For this case the channel system experiences three zones at equilibrium. The microchannels would have the same BGE concentration as in the supplying reservoir and the nanochannel would have a lower BGE concentration given by eqn (24). The only interfaces at which focusing is possible will be the two microchannel–nanochannel interfaces. Substituting eqn (24) into eqn (66) and noting $c_{0,r}^* h_r^* \gg 1$ (microchannel has low Dukhin number) leads to the following expressions for the critical mobility at different channel zones:

$$\nu_{i,r}^{*\text{crit}} = \left[1 + \frac{(1 - \nu_2^*)}{c_{0,r}^* h_n^*}\right]^{-1}, \ \nu_{i,n}^{*\text{crit}} = 1 \tag{68}$$

Note that for non-propagating CP there are no enrichment or depletion shocks, therefore, we do not distinguish between anode and cathode side reservoir regions when discussing possible focusing.

9.3.2 Propagating CP, $\nu_2^* \geq 1$

For this case the BGE concentrations are given in eqn (40) and (50). For the microchannel–nanochannel interfaces and the enrichment shock we can substitute these results into eqn (66) which yields:

$$\nu_{i,rc}^{*\text{crit}} = \frac{c_{0,r}^* h_n^*}{\nu_2^*}, \ \nu_{i,d}^{*\text{crit}} = \frac{h_n^*}{h_d^*} \frac{\nu_2^*}{2\nu_2^* - 1}, \ \nu_{i,n}^{*\text{crit}} = 1, \ \nu_{i,e}^{*\text{crit}} = \frac{2\nu_2^* - 1}{\nu_2^*} \tag{69}$$

For the depletion shock, we can substitute eqn (36) and (40) into eqn (67) to yield:

$$\nu_{i,ra}^{*\text{crit}} = \frac{2\nu_2^* - 1}{\nu_2^*}, \ \nu_{i,d}^{*\text{crit}} = \frac{\nu_2^*}{c_{0,r}^* h_d^*} \tag{70}$$

9.3.3 Propagating CP, $\nu_2^* < 1$

For this case the BGE concentrations are given in eqn (57). For the microchannel–nanochannel interfaces and enrichment shock, we can substitute these into eqn (66) resulting in:

$$\nu_{i,rc}^{*\text{crit}} = c_{0,r}^* h_n^*, \ \nu_{i,d}^{*\text{crit}} = \frac{h_n^*}{h_d^*}, \ \nu_{i,n}^{*\text{crit}} = 1, \ \nu_{i,e}^{*\text{crit}} = \nu_2^* \tag{71}$$

For the depletion shock, we can substitute eqn (57) and (58) into eqn (67) to yield:

$$\nu_{i,ra}^{*\text{crit}} = \nu_2^*, \ \nu_{i,d}^{*\text{crit}} = \frac{\nu_2^*}{c_{0,r}^* h_d^*} \tag{72}$$

10.4 Appendix IV. supplementary anionic analyte figure

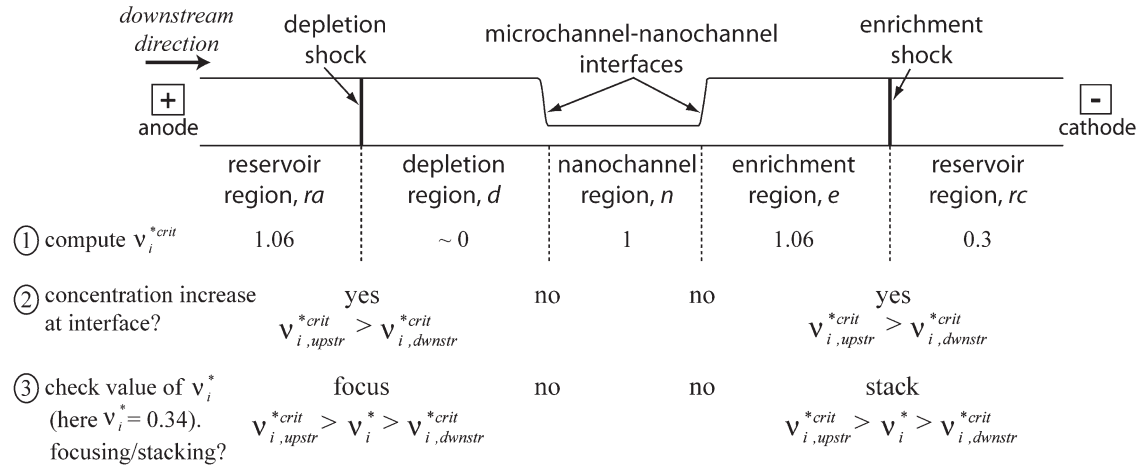

Fig. S1 Worked example of predictions for anionic analyte behavior. Step 1: Compute $\nu_i^{*\mathrm{crit}}$ for each region (reservoir, depletion, nanochannel and enrichment if propagating CP, reservoir and nanochannel if non-propagating CP) in the system. Note that $\nu_i^{*\mathrm{crit}}$ in the depletion region is lower than ν_i^* (indicated by ~ 0 in the above figure) for most practical analytes and that $\nu_i^{*\mathrm{crit}}$ in the nanochannel is unity by definition. $\nu_i^{*\mathrm{crit}}$ in the reservoir and enrichment regions depends only on the background electrolyte and channel properties. Step 2: Check for interfaces where concentration can increase by looking for higher $\nu_i^{*\mathrm{crit}}$ upstream (*upstr*) than downstream (*dwnstr*). If $\nu_{i,\mathrm{upstr}}^{*\mathrm{crit}} > \nu_{i,\mathrm{dwnstr}}^{*\mathrm{crit}}$ then anionic analytes will slow as they pass through the interface, resulting in an increase in concentration. Step 3: Check the value of ν_i^* for the analyte being considered. If $\nu_{i,\mathrm{upstr}}^{*\mathrm{crit}} > \nu_i^* > \nu_{i,\mathrm{dwnstr}}^{*\mathrm{crit}}$ then the analyte will stack or focus at the interface in question. As per the discussion in sections 6.1–6.5, anionic analytes can focus at the depletion shock or either microchannel–nanochannel interface. However, anionic analytes can only ever stack at the enrichment shock.

References

1 S. M. Kim, M. A. Burns and E. F. Hasselbrink, *Anal. Chem.*, 2006, **78**, 4779–4785.
2 T. A. Zangle, A. Mani and J. G. Santiago, *Langmuir*, 2009, **25**, 3909–3916.
3 S. J. Kim and J. Han, *Anal. Chem.*, 2008, **80**, 3507–3511.
4 R. B. Schoch, J. Han and P. Renaud, *Rev. Mod. Phys.*, 2008, **80**, 839–883.
5 Y.-C. Wang and J. Han, *Lab Chip*, 2008, **8**, 392–394.
6 A. V. Hatch, A. E. Herr, D. J. Throckmorton, J. S. Brennan and A. K. Singh, *Anal. Chem.*, 2006, **78**, 4976–4984.
7 G. B. Salieb-Beugelaar, J. Teapal, J. v. Nieuwkasteele, D. Wijnperle, J. O. Tegenfeldt, F. Lisdat, A. v. d. Berg and J. C. T. Eijkel, *Nano Lett.*, 2008, **8**, 1785–1790.
8 S. J. Kim, L. D. Li and J. Han, *Langmuir*, 2009, **25**, 7759–7765.
9 A. Plecis, C. Nanteuil, A.-M. Haghiri-Gosnet and Y. Chen, *Anal. Chem.*, 2008, **80**, 9542–9550.
10 T. A. Zangle, A. Mani and J. G. Santiago, *Eleventh International Conference on Miniaturized Systems for Chemistry and Life Sciences (μTAS2007)*, Paris, France, 2007.
11 A. Mani, T. A. Zangle and J. G. Santiago, *Langmuir*, 2009, **25**, 3898–3908.
12 F. C. Leinweber and U. Tallarek, *Langmuir*, 2004, **20**, 11637–11648.
13 I. Nischang, U. Reichl, A. Sedel-Morgenstern and U. Tallarek, *Langmuir*, 2007, **23**, 9271–9281.
14 Q. Pu, J. Yun, H. Temkin and S. Liu, *Nano Lett.*, 2004, **4**, 1099–1103.
15 A. Plecis, R. B. Schoch and P. Renaud, *Ninth International Conference on Miniaturized Systems for Chemistry and Life Sciences (μTAS 2005)*, Boston, MA, USA, 2005.
16 R. B. Schoch, L. Caprioli, A. Bertsch and P. Renaud, *Nanotech*, Montreux, Switzerland, 2005.
17 Y.-C. Wang, A. L. Stevens and J. Han, *Anal. Chem.*, 2005, **77**, 4293–4299.
18 A. Datta, J. Y. A. D. S. Gangopadhyay, H. Temkin, Q. Pu and S. Liu, *Talanta*, 2006, **68**, 659–665.
19 S. J. Kim, Y.-C. Wang, J. H. Lee, H. Jang and J. Han, *Phys. Rev. Lett.*, 2007, **99**, 044501.
20 A. Plecis, P. Svarnas and Y. Chen, *Eleventh International Conference on Miniaturized Systems for Chemistry and Life Sciences (μTAS2007)*, Paris, France, 2007.
21 R. Dhopeshwarkar, R. M. Crooks, D. Hlushkou and U. Tallarek, *Anal. Chem.*, 2008, **80**, 1039–1048.
22 D. Hlushkou, R. Dhopeshwarkar, R. M. Crooks and U. Tallarek, *Lab Chip*, 2008, **8**, 1153–1162.
23 K.-D. Huang and R.-J. Yang, *Electrophoresis*, 2008, **29**, 4862–4870.
24 K.-D. Huang and R.-J. Yang, *Microfluidics and Nanofluidics*, 2008, **5**, 631–638.
25 D. Kim, A. Raj, L. Zhu, R. I. Masel and M. A. Shannon, *Lab Chip*, 2008, **8**, 625–628.
26 K. Zhou, M. L. Kovarik and S. C. Jacobson, *J. Am. Chem. Soc.*, 2008, **130**, 8614–8616.
27 U. Tallarek, F. C. Leinweber and I. Nischang, *Electrophoresis*, 2005, **26**, 391–404.
28 M. F. A. Goosen, S. S. Sablani, H. Al-Hinai, S. Al-Obeidani, R. Al-Belushi and D. Jackson, *Sep. Sci. Technol.*, 2005, **39**, 2261–2297.
29 S. H. Chan and Z. T. Xia, *J. Appl. Electrochem.*, 2002, **32**, 339–347.
30 R. S. Foote, J. Khandurina, S. C. Jacobson and J. M. Ramsey, *Anal. Chem.*, 2005, **77**, 57–63.
31 R. J. Meagher, A. V. Hatch, R. F. Renzi and A. K. Singh, *Lab Chip*, 2008, **8**, 2046–2053.
32 J. Han, J. Fu and R. B. Schoch, *Lab Chip*, 2008, **8**, 23–33.
33 O. Bilenko, D. Bavrilov, B. Gorbovitski, V. Gorfinkel, M. Gouzman, G. Gudkov, V. Khozikov, O. Khozikov, K. Olga, N. Lifshitz, S. Luryi, A. Stepoukhovitch, M. Tcherevishinick and G. Tyshko, *Electrophoresis*, 2003, **24**, 1176–1183.
34 D. Stein, M. Kruithof and C. Dekker, *Phys. Rev. Lett.*, 2004, **93**, 035901.

35 F. Baldessari and J. G. Santiago, *J. Colloid Interface Sci.*, 2008, **325**, 539–546.
36 R. B. Schoch, H. van Lintel and P. Renaud, *Phys. Fluids*, 2005, **17**, 100604.
37 J. Lyklema, *Fundamentals of Interface and Colloid Science, Solid-Liquid Interfaces*, Academic Press, London, 1995, vol. II.
38 D. Burgreen and F. R. Nakache, *J. Phys. Chem.*, 1964, **68**, 1084–1091.
39 S. S. Dukhin and V. N. Shilov, *Kolloidnyi Zhurnal*, 1969, **31**, 706–713.
40 M. Block and J. A. Kitchener, *J. Electrochem. Soc.*, 1966, **113**, 947–953.
41 I. Rubinshtein, B. Zaltzman, J. Pretz and C. Linder, *Russ. J. Electrochem.*, 2002, **38**, 853–863.
42 I. Rubinstein and B. Zaltzman, *Phys. Rev. E: Stat. Phys., Plasmas, Fluids, Relat. Interdiscip. Top.*, 2000, **62**, 2238–2251.
43 B. Zaltzman and I. Rubinstein, *J. Fluid Mech.*, 2007, **579**, 173–226.
44 A. Höltzel and U. Tallarek, *J. Sep. Sci.*, 2007, **30**, 1398–1419.
45 S. Y. Park, C. J. Russo, D. Branton and H. A. Stone, *J. Colloid Interface Sci.*, 2006, **297**, 832–839.
46 T. Postler, Z. Slouka, M. Svoboda, M. Přibyl and D. Šnita, *J. Colloid Interface Sci.*, 2008, **320**, 321–332.
47 R. Bharadwaj, D. E. Huber, T. K. Khurana and J. G. Santiago, in *Handbook of Capillary and Microchip Electrophoresis and Asociated Microtechniques*, ed. J. P. Landers, CRC, Boca Raton, 3rd edn, 2008, pp. 1085–1120.
48 B. J. Kirby and E. F. Hasselbrink, *Electrophoresis*, 2004, **25**, 187–202.
49 B. J. Kirby and E. F. Hasselbrink, *Electrophoresis*, 2004, **25**, 203–213.
50 S. M. Kuo, S. J. Chang and Y. J. Wang, *J. Polym. Res.*, 1999, **6**, 191–196.
51 J.-O. You and D. T. Auguste, *Biomaterials*, 2008, **29**, 1950–1957.
52 S. Ge, B. Yi and P. Ming, *J. Electrochem. Soc.*, 2006, **153**, A1443–A1450.
53 Y. Daiko, K. Katagiri and A. Matsuda, *Chem. Mater.*, 2008, **20**, 6405–6409.
54 R. D. Chambers and J. G. Santiago, *Anal. Chem.*, 2009, **81**, 3022–3028.
55 A. Persat, M. E. Suss and J. G. Santiago, *Lab Chip*, 2009, **9**, 2454–2469.
56 T. A. Zangle, PhD thesis, Stanford University, 2010.
57 A. E. Herr, J. I. Molho, K. A. Drouvalakis, J. C. Mikkelsen, P. J. Utz, J. G. Santiago and T. W. Kenny, *Anal. Chem.*, 2003, **75**, 1180–1187.
58 S. Song and A. K. Singh, *Anal. Bioanal. Chem.*, 2006, **384**, 41–43.
59 J. H. Lee, Y.-A. Song and J. Han, *Lab Chip*, 2008, **8**, 596–601.
60 J. H. Lee, Y.-A. Song, S. R. Tannenbaum and J. Han, *Anal. Chem.*, 2008, **80**, 3198–3204.
61 S. Levine, J. R. Marriott and K. Robinson, *J. Chem. Soc., Faraday Trans. 2*, 1975, **71**, 1–11.
62 R. Karnik, R. Fan, M. Yue, D. Li, P. Yang and A. Majumdar, *Nano Lett.*, 2005, **5**, 943–948.
63 T. Hirokawa, M. Nishino, N. Aoki, Y. Kiso, Y. Sawamoto, T. Yagi and J.-I. Akiyama, *J. Chromatogr., A*, 1983, **271**, D1–D106.
64 D. Milanova, R. D. Chambers and J. G. Santiago, 2010, manuscript in preparation.
65 R. Bharadwaj, J. G. Santiago and B. Mohammadi, *Electrophoresis*, 2002, **23**, 2729–2744.